# Energy transfer in the system of PbS quantum dots

**School of Electrical Engineering**

Thesis submitted for examination for the degree of Master of Science in Technology.

Espoo 19.07.2016

**Thesis supervisor:**
Associate Professor Markku Sopanen

AALTO UNIVERSITY
SCHOOL OF ELECTRICAL
ENGINEERING

ABSTRACT OF THE
MASTER'S THESIS

Author: Tatiana Vorsina

Title: Energy transfer in the system of PbS quantum dots

Date: 19.07.2016 Language: English Number of pages: 51

Department of Micro- and Nanosciences

Professorship: S - 104

Supervisor: Associate Professor Markku Sopanen

This work is devoted to the investigation of the process of Förster resonant energy transfer between lead sulphide quantum dots of different size in the porous matrix and on the glass surface at both room and decreased temperatures. As a result, we observed quenching of photoluminescence (PL) for donors together with flare-up of PL of acceptors, which was accompanied by significant increasing of lifetimes of acceptors up to values characteristic for donors. This unexpected effect can be explained using three-level model which is based on a complex energy structure of PbS quantum dots-donors, which are involved in the energy transfer. The observed effect can lead to a significant change in the dynamic characteristics of the charge carriers in quantum dot solar cells.

Keywords: quantum dots, energy transfer, solar cells

## Preface

I wish to thank Prof. Dr. Alexander Baranov, Prof. Dr. Anatoly Fedorov, Dr. Alexander Litvin, and all my colleagues from the department of Optical Physics and Modern Natural Science at ITMO University for all their support during my Master's studies.
I also thank Prof. Markku Sopanen for his supervision and support during the two semesters I spent at Aalto University in Finland.

# Contents

## Symbols and abbreviations

### Symbols

$A_0$, $A_1$, $A_2$, $A_3$ constant coefficients

$a_{exc}$ Bohr radius of the exciton

$A, B$ coefficients

$C$ the molar concentration

$D$ optical density

$d_{av}$ average diameter

$E$ efficiency of energy transfer

$e$ elementary charge

$E_g$ energy gap

$\hbar$ Planck's constant

$\hbar\omega$ energy of incident radiation

$I$ intensity of the incoming beam

$I_{ov}$ overlapping integral

$I_0$ intensity of the passed beam

$I_D$ donor luminescence intensity without the acceptors

$I_{DA}$ donor luminescence intensity in the presence of acceptors

$I_D^H$ quantum spectral density of the luminescence radiation

$k$ coefficient of proportionality

$k_B$ Boltzmann constant

$k_T$ velocity constant

$l$ the optical path length

$n$ ratio of PL quenching

$N_0$ concentration at the initial moment

$R$ radius of quantum dot

$r$ distance between the donor and the acceptor

$R_0$ Förster's radius

$r_{crit}$ critical radius of the nuclei

$S$ degree of solution supersaturation

$T$ temperature

$t$ decay time of PL

$t_1$, $t_2$, $t_3$ time parameters

$t_{long}$, $\tau_{long}^{D}$ long time-components

$t_{short}$, $\tau_{short}^{A}$ short time-components

$U$ rate of nucleation

$V$ the molecular volume

$V_m$ molar volume

$\gamma$ the specific interface energy

$\Delta G$ change of Helmholtz free energy

$\varepsilon$ diectric permittivity

$\varepsilon$ extinction coefficient

$\varepsilon_A$ extinction coefficient

$\lambda$ wavelength

$\mu$ reduced mass of the exciton

$\nu$ wave number

$v_s$ concentrations of saturated solution

$v_s$ concentrations of supersaturated solution

$\tau_d$ lifetime of excited state for the donor in absence of the acceptor

$\tau_D$ donor lifetime in a pure sample

$\tau_{DA}$ donor lifetime in the presence of the acceptor

**Abbreviations**

*AFM* atomic force microscopy

*FRET* Förster resonance energy transfer

*IR* infrared

*MPA* 3-mercaptopropionic acid

*QD* quantum dot

*PL* photoluminescence

*UV* ultraviolet

## 1. Introduction

The future of mankind is tightly bound to both rational use of natural resources and to development of alternative sources of energy which contribute to the electric energy generation more and more year after year [1]. For instance, in 2013 one fifth of the global energy demand was provided by renewable sources of energy where solar energy played a considerable role [2]. At present day, production of solid state photoelectric cells is a costly process and does not always ensure success compared to the conventional technologies in power industry. For this reason, it is particularly topical now to find new materials and technologies which would reduce the cost of solar cells production.

A successful solution which provides a desirable compromise between efficiency and cost of production is an innovative technology of solar cell spray developed in 2014 at Toronto University [3]. The SprayLD system is based on spraying colloidal quantum dots (QD) on flexible and irregular surfaces which turns them into solar panels. Such a method allows designing large area solar cells that are technically challenging and unprofitable for silicon-based solar cells. Dependence of QD energy gap width from its geometry allows new photocells to absorb radiation in various bands of solar spectrum from ultraviolet (UV) to infrared (IR) range as opposed to traditional semiconductor materials which absorb only within a very narrow spectral range.

The ability of efficient absorption within a wide spectral range covering almost the whole spectrum of sun radiation is characteristic for lead sulphide (PbS) QDs which consequently have been chosen for the research in this thesis. Besides, colloidal solution of PbS QDs may serve as photoelectric material both in ink-jet printing [4] and in roll-to-roll technology [5], and in the SprayLD spray system, which reflects the importance of the topic chosen.

The paper objective is to study fundamental phenomenon of induction-resonance nonradiative energy transfer (FRET) between lead sulphide QDs of different sizes. This process may influence the efficiency of converting solar radiation into electric energy. That is why understanding its qualities may result in improvement of the technologies existing in solar energetics.

## 1. Characteristics, synthesis and application of colloidal quantum dots

### 2.1 Colloidal quantum dots

A quantum dot means any three-dimensional potential energy well which is accompanied by the energy spectra quantum size effect. Nanocrystals are conventionally understood as quantum dots limited by any matter different from the one they are produced from [6]. In this case presence of heterointerfaces leads to formation of three-dimensional spatial delimitation or confinement. Beside heterointerfaces, mechanical stresses and deviations of semiconductor layer thickness also result in spatial delimitation of electrons, holes and excitons motion.

There are excitons within semiconductor which represent bound state of electrons and holes, have a radius considerably exceeding interatomic spaces due to high dielectric permitivity and, consequently, faint electrostatic interaction. Therefore, peculiar spatial scale of an exciton within the semiconductor in ground state with $n=1$ may be estimated as effective Bohr radius [7]:

$$a_{exc} = \frac{\varepsilon \hbar}{\mu e^2} \tag{1}$$

Thus, the fullest definition of a quantum dot may be defined in the following way: a quantum dot is a semiconductor nanocrystal with characteristic dimensions approximately equal to exciton radius, where charge the motion of the carriers is limited in all three dimensions. Thus, electrons and holes are localized in a three-dimensional potential energy well.

We now proceed to review the colloidal QDs class. Colloidal QDs represent semiconductor nanocrystals, in most cases coated with organic molecules which play a role of a stabilizer. Colloidal QDs generally consist of a considerable number of atoms, about $10^3$-$10^5$ of atoms, and have a diameter lying in the range from 2 μm to 10 μm.

Figure 2.1 represents a colloidal QD model with a semiconductor nucleus and organic coating.

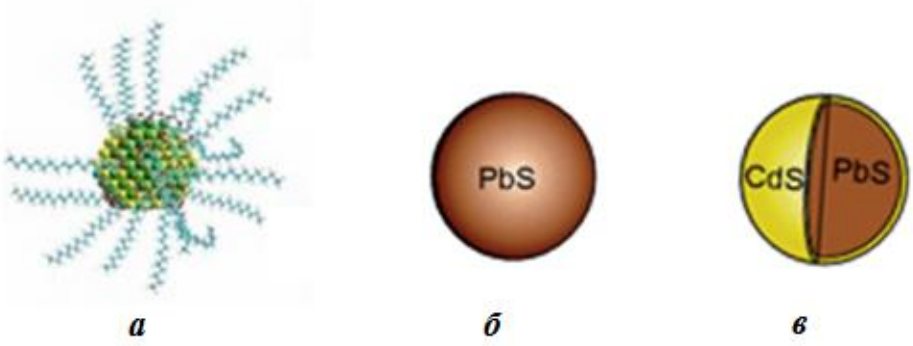


Figure 2.1 – a) PbS QD model for the colloidal core-shell [5], b) PbS QD without the shell and c) PbS-CdS of the core-shell type without the organic molecules [8].

Colloidal QDs are characterized by composition, size, and shape [9]. QDs functioning as a basis for effective photoluminescence (PL) shall be based on a material with a direct band character of the spectrum. Depending on the energy gap the semiconductor materials may be subdivided:

a) Wide-band – UV band,

b) Medium-band – visible band,

c) Narrow-band – near IR band (0.9 μm - 1.7 μm) PbS QDs belong to this class.

QDs may have a spherical, ellipsoid, or cubical shape, as well as have a complex geometry, for example, a truncated parallelepiped shape [8]. A sphere is an idealized shape, since the QDs actually have a more complex shape which may be claimed to be a sphere only in certain approximation. The spherical QDs happen to have wider practical application and turn up to be easier in production. In most cases, spherical QDs are produced by means of colloidal synthesis.

Quantum dots may also be multicomponent dots which include:

1) Alloyed ones,

2) QDs based on solid solutions,

3) QDs based on a heterojunction:

- Type 1 – when the nucleus is a narrow-band semiconductor with the energy gap inside that of the host material.
- Type 2 – when both the nucleus and the coating have energy gaps with staggered alignment against each other.

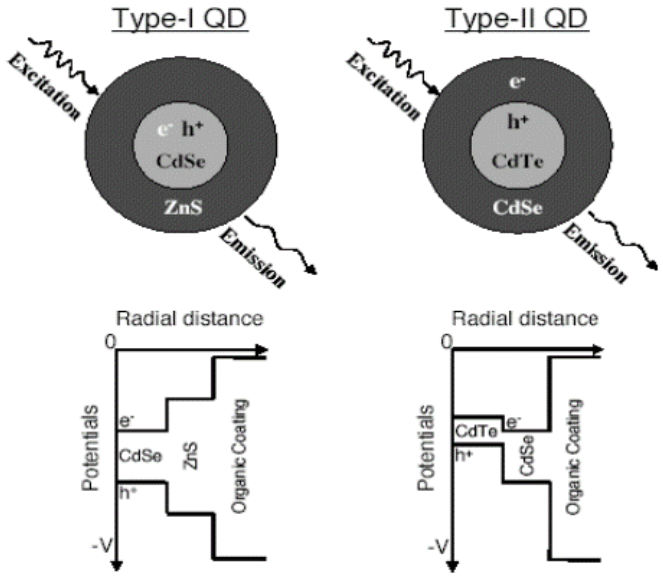


Figure 2.2 – CdTe-CdSe based colloidal quantum dots with heterojunctions of (a) type 1 and (b) type 2.

## 2.2 Confinement effect

Restriction of charge carriers' mobility within a QD resulting in its energy spectrum transformation displays the fact that physical properties depend on geometrical dimensions of the system. This phenomenon is called a spatial quantization effect and lies in the fact that linear contraction of the system or its elementary excitations (excitons) leads to considerable modification of its energy spectrum: a quasi-continuous spectrum becomes discrete.

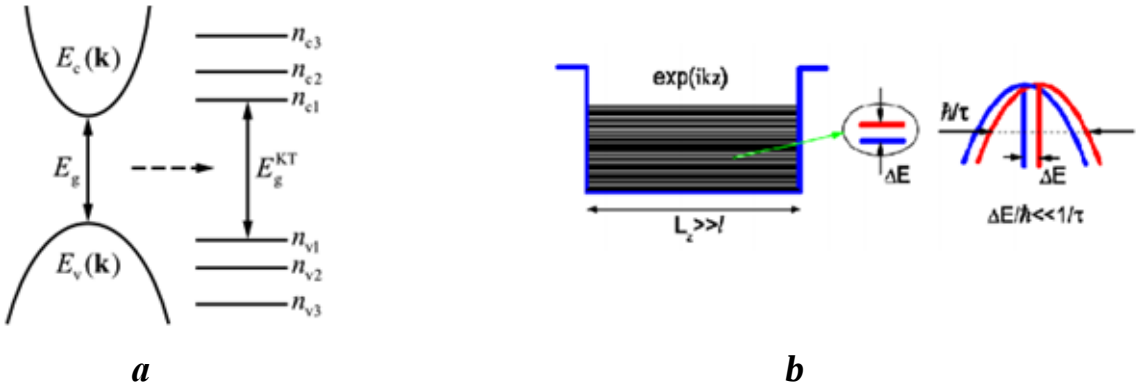


***a*** ***b***

Figure 2.3 – a) transformation of quasi-continuous spectrum of a 3D semiconductor into discrete spectrum of a QD and b) quasi-continuous spectrum in a 3D material.

Discreteness of the spectrum or size quantization of the electron and hole states leads to displacement of optical lines within absorption spectra depending on the nanocrystal radius [8]. This phenomenon has been experimentally observed for semiconductors of various groups [7]. In such a way, electro-optical properties depend on the nanocrystal size, more specifically, on its radius *R*. The second key parameter, which determines quantum size effects of an electron-hole pair, is an effective Bohr radius of the exciton, $a_{exc}$.

Depending on the correlation of these two values, various localization modes of charge carriers within QDs may be identified:

1) Weak mode - $R/a_{exc} > 4$,
2) Strong mode - $R/a_{exc} < 2$,
3) Intermediate mode - $2 < R/a_{exc} < 4$.

In the mode of weak confinement, the electron-hole pair behaves as an exciton but in this case its center of mass motion will be quantized.

In the mode of strong confinement, separate quantization of the kinetic motion of electron and hole takes place. It results in a distinct discrete structure of energy levels which results from the fact that the interaction of an electron and a hole with a delimited crystal considerably outweighs its

electrostatic interaction. In the mode of strong confinement, carriers may be considered independent.

Intermediate mode is the least studied due to lack of experimental data opposed to the two extreme cases.

In such a way different modes of confinement may be realized for the same QD system depending on their size, whereas lead sulphide QDs for the particular band fall into the strong confinement mode.

For example, let us look at the absorption spectra of five colloidal solutions of QDs from CdSe nanocrystals with various radiuses: 1.2, 1.7, 2.3, 2.8 and 4.1 μm [10]. Peculiarities relating to the interband optical transitions connected with different electron and hole states can be clearly seen on the spectra. For example, the first two absorption bands are conditioned by transitions $1S \rightarrow 1S_{3/2}$ and $1S \rightarrow 2S_{3/2}$.

Convergence of the absorption spectra of nanocrystals at high energies ħω to absorption spectra of 3D material demonstrates that, in the case of high energies, optical absorption of samples stops being dependent on nanocrystal dimensions and is governed exclusively by the used semiconductor material.

The observed spreading of bands which complicates absorption spectra analysis is a result of dimensional dispersion in colloidal solutions. That is why it is so important to synthesize monodispersed colloidal solutions.

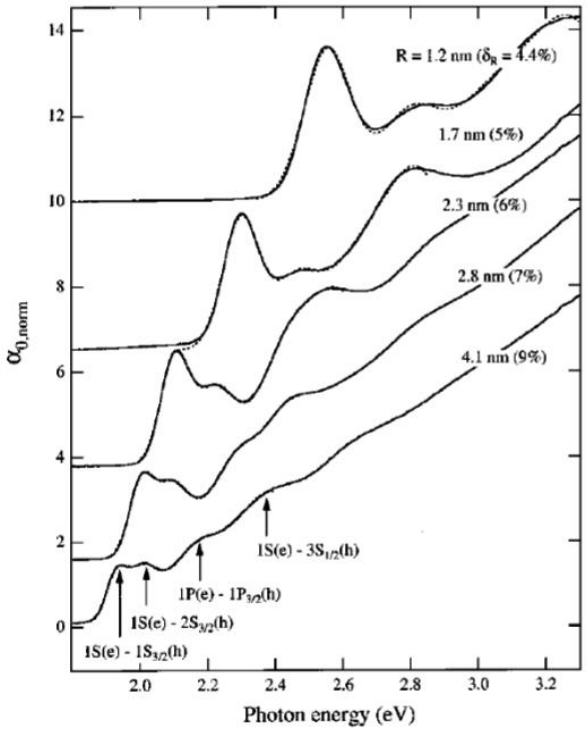


Figure 2.4 – Absorption spectra of CdSe nanocrystals with radii from 1.2 μm to 4.1 μm. [10]

## 2.3 Transfer of energy between quantum dots

Phenomenon of nonradiative energy transfer between QDs in colloidal solution is a fundamental process which represents one of the key factors influencing efficiency of solar panels based on colloidal QDs. Nonradiative Förster excited state energy transfer from a donor to an acceptor which occurs without photons emission and by its nature refers to dipole-dipole interaction. QDs of different size serve as donor-acceptor pair. Transfer of energy may be presented as a sequence of processes:

1) Transition into excited state of the donor after laser excitation.
2) Vibrational relaxation of the donor in excited state.
3) Transfer of the excited state energy from donor to acceptor.
4) Vibrational relaxation within the acceptor.
5) Emission from the acceptor.

The whole process is illustrated in figure 2.5.

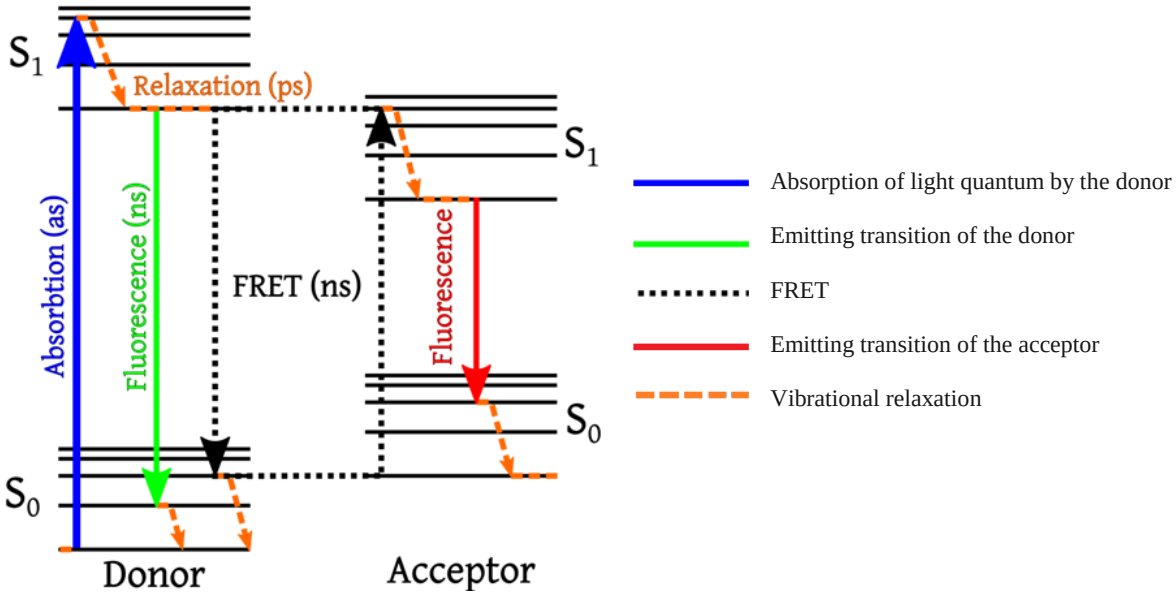


Figure 2.5 – Scheme of energy transfer according to the FRET mechanism, where arrows stand for main transitions.

Förster's theory states that for efficient transition of energy from a donor to an acceptor the following two conditions shall be simultaneously achieved [11].

1) Acceptor's absorption spectrum and donor's luminescence shall be overlapped in the way that overlapping integral be not equal to zero:

$$I_{ov} = \int I_D^H(\nu) \cdot \varepsilon_A(\nu) \cdot \nu^{-4} \cdot d\nu \neq 0 \quad (2)$$

2) Distance between the donor and the acceptor shall not exceed the Förster's radius value $R_0$ wherein energy transfer efficiency equals to 50%, or such transfer will be inefficient.

Velocity constant of energy transfer within one selected donor-acceptor pair is governed by the expression:

$$k_T = \frac{1}{\tau_d}\left(\frac{R_0}{r}\right)^6 \quad (3)$$

where $\tau_d$ is the excited state lifetime of the donor in absence of the acceptor, $r$ is the distance between the donor and the acceptor, $R_0$ is the Förster's radius. Efficiency of energy transfer may be estimated by Förster's formula, presented in [12]:

$$E = \frac{R_0^6}{R_0^6 + r} \quad (4)$$

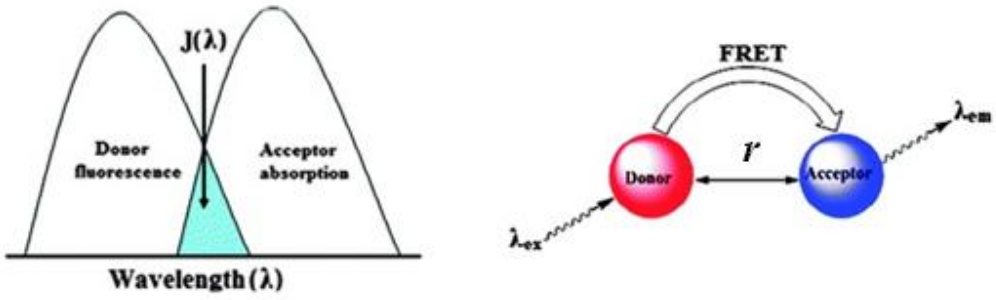


Figure 2.6 – Illustration of two conditions necessary for transfer of energy according to the FRET mechanism. [13]

## 2.4 Synthesis of colloidal quantum dots

There are many various ways to synthesize colloidal QDs. However, due to a relatively recent development of these methods (from 1990-s, and active development at present day) there are some difficulties with classification resulting from constant modification of methods. Most common division of synthesis methods is a division by the type of construction of the nanostructures posing two main approaches:

1) "Top-down" approach which is based on getting the nanoscale objects from 3D materials by means of fragmentation and atomization (mainly mechanically).

2) “Bottom-up” approach based on natural physical, chemical and biological processes which result in formation of complex nanoscale objects from separate molecules or ions. Generally these methods are connected with the use of complex equipment needed for keeping high-vacuum, controlled-temperature conditions and other parameters exercising a decisive influence on growth of samples.

On the whole, “bottom-up” methods are more complex and require more time compared to “top-down” methods. Though they allow synthesizing higher quality nanostructures containing minimum defects and contaminations and with narrow size distribution, i.e., give a chance to grow monodisperse assemblages.

## 2.5 Hot injection synthesis method

Below we will discuss in more detail one of the bottom-up methods, which turned out to be the most successful among the colloidal chemical methods of synthesis, and which allows growing monodisperse colloidal QDs. This is the growth method in non-polar media developed by Murray in 1992 [15], and it has a number of significant advantages:

a) The ability to control the growth process of the QDs, for example, by varying temperature.

b) The ability of receiving QDs in the form of powder and absence of matrices, which greatly simplifies the process of QD purification.

c) A narrow distribution of the geometric parameters of the QDs:

- About 5% for $A^2B^6$ elements;
- About 10% for $A^3B^5$ elements;

d) Relatively low process temperatures and, consequently, the absence of complex equipment.

This method is also known as the hot injection method because of the fact that it is based on the following procedure: components containing chemicals with elements of the selected groups are injected in a hot, continuously stirred dispersion medium. As a result, there is a fast reaction and formation of locally supersaturated solution, leading to the process of forming nuclei of solids, i.e. nucleation [16].

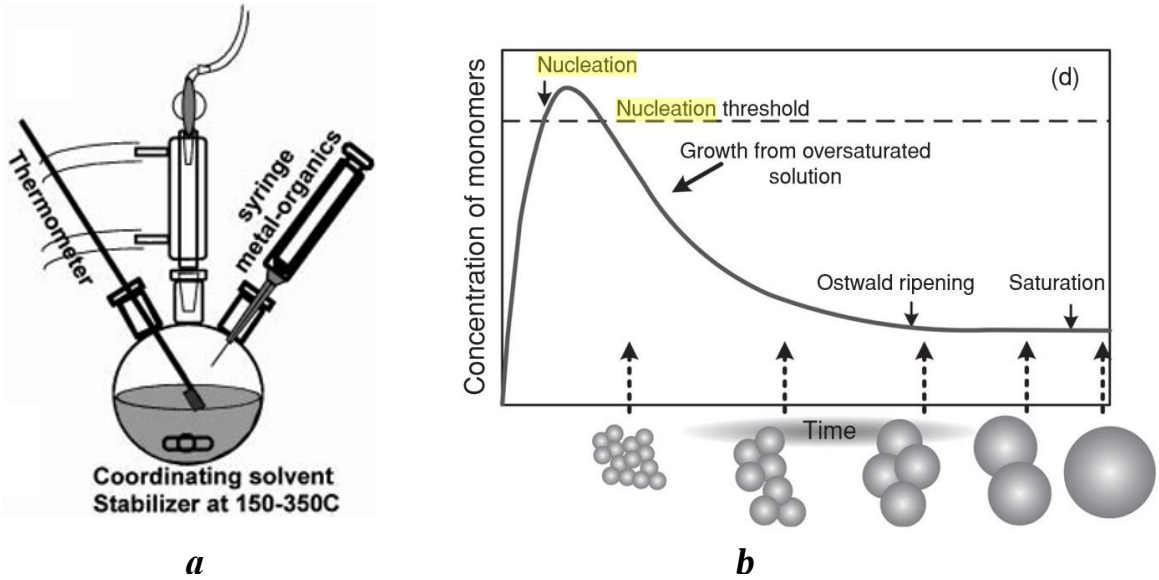


***a*** ***b***

Figure 2.7 - a) Schematic of the hot injection method [16] and b) the concentration of the condensed agent at the nucleation stages and growth from a highly supersaturated solution.

Nucleation is followed by the growth of the nuclei and Ostwald ripening stage. We describe the basic physical processes that are present in each of the three stages [9].

1) *Nucleation in the supersaturated solution*

According to the theory, nucleation has a spontaneous nature and is based on an ability of molecules and ions introduced in the solution to get crystallized and form nuclei in unstable areas of the supersaturated solution. The rate of nucleation is described by the following equation:

$$U = kS = k(v_{ss} - v_s)/v_s \tag{5}$$

where k is a coefficient of proportionality, S is the degree of supersaturation and $v_s$, $v_{ss}$ are the concentrations of the saturated and the supersaturated solutions, respectively.

The larger the value of relative supersaturation $(v_{ss} - v_s)/v_s$, the faster nucleation occurs, which means that more crystallization centers appear leading to a deviation decrease in particle sizes from an average value. In the process of nucleation a new phase interface appears, which leads to an increase in the free energy of the system. Simultaneously, the system energy decreases because of chemical transformations.

The total change in the free system energy is described by the expression:

$$\Delta G = \Delta G_{incr} + \Delta G_{decr} = 4\pi r^2 \cdot \gamma - \frac{4}{V}\pi r^3 k_B T \cdot \ln S \tag{6}$$

where $r$ is the nuclei radius, $k_B$ is the Boltzmann constant and $\gamma$ is the specific interface energy.

Thus, at a certain critical size of the nuclei $r_{crit}$ the function describing the total change in free energy has a point of extremum:

$$r_{crit} = \frac{2V\gamma}{3k_B T \ln S} \tag{7}$$

The maximum value of free energy corresponds to the activation energy for nucleation. From this equation it follows that nuclei of a smaller size are formed in the supersaturated solution. For the solution with a certain degree of supersaturation S all particles of the size larger than the critical size will grow, and the rest will be dissolved.

2) *Growth of nuclei*

Within the colloidal theory the link between the crystal shape and the interface energy of its facets is considered, from which it follows that the rate of forming crystal facets is high and is determined solely by the rate of diffusion. Temperature is the basic governing parameter in the diffusion processes. Assuming that the process of the facet growth is slower than the process of supplying the substance, the variation law for the concentration of a substance, such as cadmium, can be written as:

$$\frac{d[Cd]_t}{dt} = -kA(t)[Cd]_t\, N(t) \tag{8}$$

Then the growth of nanocrystal radius if assuming spherical shape is described by the formula:

$$\frac{dr}{dt} = k\left(V_m\left([Cd]_0 - [Cd]_{eq}\right) - \frac{N_0 4\pi r^3}{3}\right) = k(A - Br^3) \tag{9}$$

This formula is good for approximating the experimental data, which can be seen in the Figure 2.9 containing data on the growth of CdSe ($A^2B^6$) QDs [17].

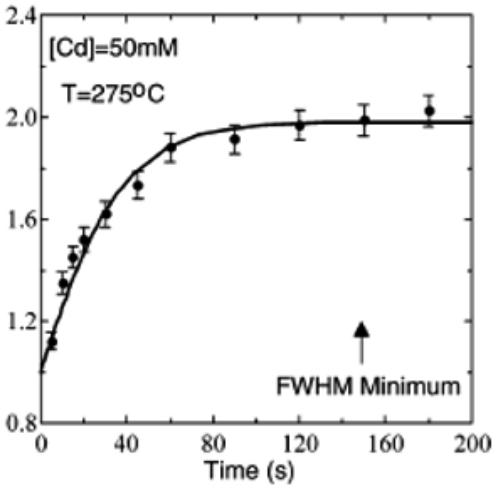


Figure 2.8 - Dependence of the size of the CdSe nanocrystals on the growth time. [17]

3) *Ostwald ripening stage*

In the later time of the system development when the reagents have been exhausted and the nucleation stage is completed, the process of Ostwald ripening begins. This process is characterized by the growth of large particles due to the dissolution of the smaller ones, and the interface energy of the system is reduced due to the dissolution of fine particles having a large surface area in total.

Every moment of time is characterized by the value of the critical radius which increases with the decrease in the supersaturated solution. Particles with sizes greater than the critical value at a given time continue to grow according to the macroscopic laws.

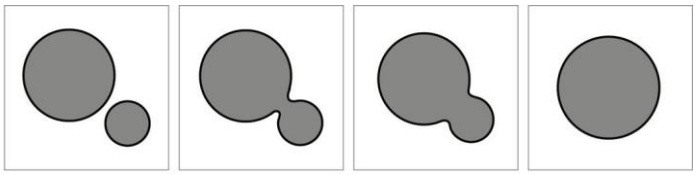

Figure 2.9 - Successive stages of Ostwald ripening.

The above processes and their respective physical models underlie the growth of monodisperse colloidal QD systems within the hot injection method.

## 2.6 Applications of quantum dots

The dependence of the energy spectrum on the size gives a great potential for the practical use of colloidal QDs, which are increasingly used in various fields from semiconductor devices to medical applications and cryptographic security systems. QDs can be considered as an active medium for lasers and as a material for LEDs, fluorescent labels and displays that have already been put into commercial production. Every year the number of applications and technologies based on QDs increases with the growth of research interest to them, as shown by the growth of the QD market.

Another QD feature important in terms of practical use is the ability to exist in the form of sols, which makes it easy to obtain coverage from QDs films with such cheap methods as spin-coating [5] and ink-jet printing [4], which allow avoiding the use of expensive vacuum technologies applied for the production of microelectronic devices and silicon solar cells. Since the main application field of colloidal QDs is photovoltaics, below we will give a brief overview of solar cells with the basic directions of their development, and we will consider examples of the most successful technologies.

## 2.7 Nanostructures in solar energy

Currently, among all kinds of solar cells elements based on crystalline silicon, with a lifetime of 25 years and the efficiency of 25.6% [26], which is close to the theoretical limit of 32% [27], are still dominating. This type of solar cell refers to the elements of the first generation, the origin of which is dated to 1950s. Elements of the second generation are based on amorphous or polycrystalline silicon, and characterized by a simple production technology and, consequently, lower production cost. Their efficiency is much lower than that of the first generation elements [26].

In contrast to the elements of the first and second generation, elements of the third generation include many designs based on the use of various technologies. One of the directions is the use of nanostructures as the core element in the third generation solar cells. The cost of energy produced by the third generation elements is significantly lower than that of the previous generations.

Among the technologies based on the use of nanostructures, we can distinguish three main groups of solar cells:

1) Photo-electrochemical dye-sensitized solar cells [28],
2) Polymer solar cells,
3) Solar cells based on colloidal QDs.

*Dye-sensitized solar cell*

1) Description

The element consists of a semiconductor anode and metal cathode immersed in an electrolyte. A film 10 μm thick, composed of $T_iO_2$ particles having a diameter of about 15 nm, sensitized with a dye monolayer, acts as an anode. Using a highly porous material, nanocrystalline $T_iO_2$, allows increasing the absorbent surface area 780 times compared to a flat anode [28], resulting in a significant increase in the share of absorbed photons.

2) Operating principle

When dye molecules absorb photons, an electron is transferred from the ground to the excited state, and moves to the $T_iO_2$ conduction band for a time of about $10^{-15}$ seconds. Further, electron diffuses through the $T_iO_2$ film, reaching a glass electrode, and flows through the conductor to the second electrode. The dye molecule is reduced, yielding an electron from the iodide ion, which turns into the iodine molecule and diffuses to the back-electrode, from which it receives an electron and becomes again the iodine ion.

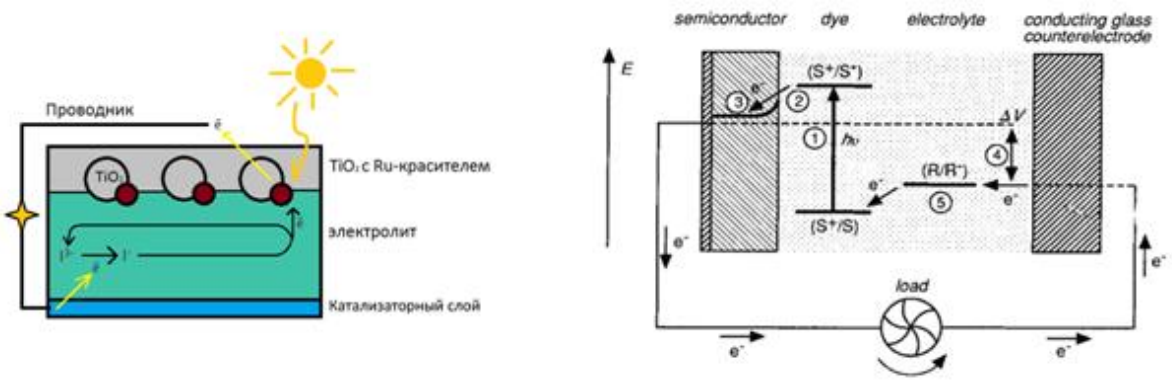


***a*** ***b***

Figure 2.10 - a) Operating principle of the dye-sensitized solar cell and b) the system of energy levels in each phase. [28]

Thus, the dye-sensitized solar cell is commercially attractive due to the simplicity, low production cost and thermal stability. It also has an efficiency of 10-12% limited to the theoretical value of 33% [29].

*The polymer solar cells*

1) Description

A solar cell consists of thin polymer films inflicted layer-by-layer with different functions. The photoactive layer composed of the p- and n-type organic semiconductor where electron-donors are conjugated polymers and electron-acceptors are $C_{60}$ fullerenes and derivatives thereof.

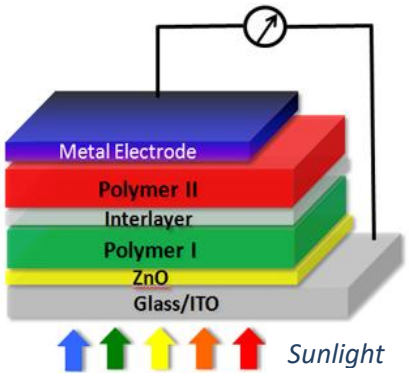


Figure 2.11 - Order of layers in the polymer solar cell.

2) Operating principle

The operating principle of polymer solar cells makes up photo-induced charge separation between electron-accepting and electron-donor materials of the photoactive layer, which provides

the generation and efficient transport of charge carriers to both electrodes [30]. The operating principle of the polymer solar cells can be represented as a sequence of the following physical processes:

1) When absorbing photons excitons are generated in the photoactive layer. Then they move to the p- and n-type semiconductor interface, where exciton dissociation takes place.

2) After the exciton dissociation, the electron and the hole remain connected, with the exciton transiting to the acceptor, and the hole remaining in the donor phase. Such a system is called a charge transfer complex, and can get either completely separated or recombined.

3) In the case of dissociation the electron and the hole migrate to the respective electrodes, moving only in its phase, so it is important to form continuous channels throughout the photoactive layer.

4) The final stage is the process of electrodes collecting charges, which is hindered by potential barriers and recombination processes. In this connection, buffer layers are used to minimize these two effects.

The polymer and fullerene solar cells can be applied to flexible surfaces, and may be obtained by printing as well [5], which greatly reduces their production cost. Furthermore, they have an efficiency of approximately 10% and are environmentally safe, but are prone to degradation.

*Solar cells based on colloidal QDs*

In addition to the unique physical properties QDs have the ability to be integrated in the liquid-phase technologies, such as roll, printing and SprayLD [3], which greatly simplifies the solar cell production process and makes it economically attractive. This combination of practical and fundamental properties makes QDs a desirable object of study and explains the variety of designs of solar cells, among which there are the following groups:

- ✓ On the basis of Schottky contact (metal / semiconductor transition).
- ✓ With heterojunction (conjugated polymer / quantum dot [31]).
- ✓ Sensitized quantum dots.

Despite the fact that devices based on QDs haven't got efficiency values comparable to silicon cells yet, the given industry is rapidly developing and there is every reason to believe that higher efficiency values will be obtained soon.

We will consider the factors that play a key role in increasing the efficiency of such solar cells. First, in the colloid synthesis process quantum dots are covered with the molecules of surface-active

agents (surfactants) to prevent coagulation, and the important step is to replace the original stabilizer for new surface ligands, whose usage reduces the distance between QDs, and hence helps to increase the charge mobility. The correct choice of ligands can significantly increase the conductivity between QDs layers. Secondly, photons of solar radiation are in the energy range from 0.5 eV to 3.5 eV, and those whose energy exceeds the $E_g$ value of semiconductor QDs lead to the appearance of hot charge carriers. Thanks to the discrete structure of QDs energy spectrum, hot charge carriers can lead to multi-exciton generation, which minimizes heat losses, which make up almost half of all losses in solar cells [29].

For example, in PbSe QDs with $E_g$ = 0,636 eV we observed the generation of seven excitons at absorbing a photon with energy $h\nu = 7,8E_g$ [32].

## 2.8 SprayLD Technology

After analyzing the evolution of the solar cells, it can be concluded that at this stage there is a tendency to reduce the device production cost and to simplify production process sometimes even to the detriment of efficiency.

Under such conditions, the methods that, first, meet these two criteria, and secondly, are applicable in large-scale industrial products bring the greatest advantage. At present, a large number of methods and technologies of producing solar panels on QDs have been developed, but many of the technologies, such as spin-coating and dip-coating are limited to the laboratory scale [33].

In contrast to these methods, colloidal SprayLD sputtering technology of QDs allows creating solar cells with efficiency values of 8.1% [3] on the commercial scale. The authors have developed a fully automated system based on sputtering and depositing QDs with an average size of 20 nm on specially prepared substrates. Rational use of colloidal QDs is caused by several facts. Firstly, colloidal QDs are precipitated from a liquid medium in which they remain stable for a long time, and thus are suitable for inexpensive large-scale production, and, secondly, because QDs are produced SprayLD under controlled growth conditions, it greatly simplifies the morphological and chemical control in subsequent coating processes. However, it requires careful control of spray characteristics. The schematic of a colloidal QD spraying tool is presented in Figure 2.14.

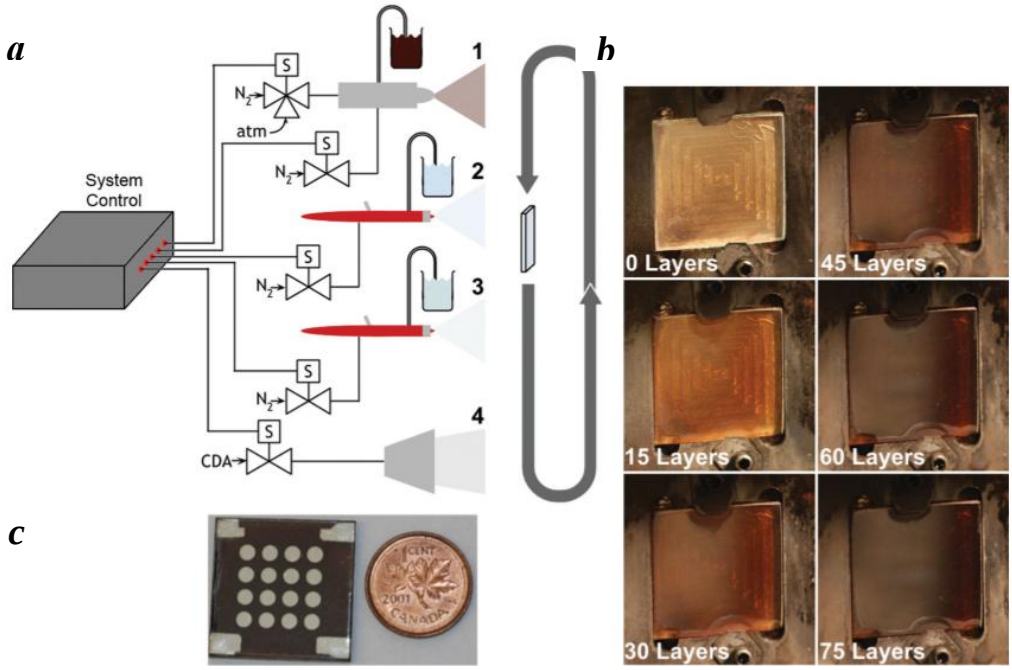


Figure 2.12 – a) Full setup of layer-by-layer spray deposition. Stage 1 involves the fine mist spraying of colloidal QDs. Stages 2 and 3 use commercial air brushes to spray MPA diluted in methanol and pure methanol, respectively. In stage 4, an air blade applies a curtain of high pressure compressed dry air to aid in drying the solvent; b) A time-lapse series of photos of a square fl uorine-doped tin oxide coated glass substrate as it is sprayed with the number of sprayLD layers and c) a photograph of a sprayLD sample with 166.7 $mm^2$ devices. [3]

A complete cycle of SprayLD method consists of the following steps:

1) Synthesis of PbS QDs with the participation of $CdCl_2$.
2) Preparation of the substrate to be sprayed.
3) Spraying and depositing QDs on the substrate.
4) Analysis of the main characteristics of the sample.

To analyze the resulting structures the atomic force microscopy (AFM) is used, as well as a number of photovoltaic measurements performed to make sure the high quality of the sample.

As can be seen from the comparative analysis of spraying QDs via SprayLD method and with spin-coating methods gives more durable and smooth films. A more detailed analysis of the samples is presented in reference [3].

Thus, the method of spraying colloidal QDs with the SprayLD technology is a successful example in the production of the third generation solar cells due to low cost and simplicity, which can be used on the industrial scale.

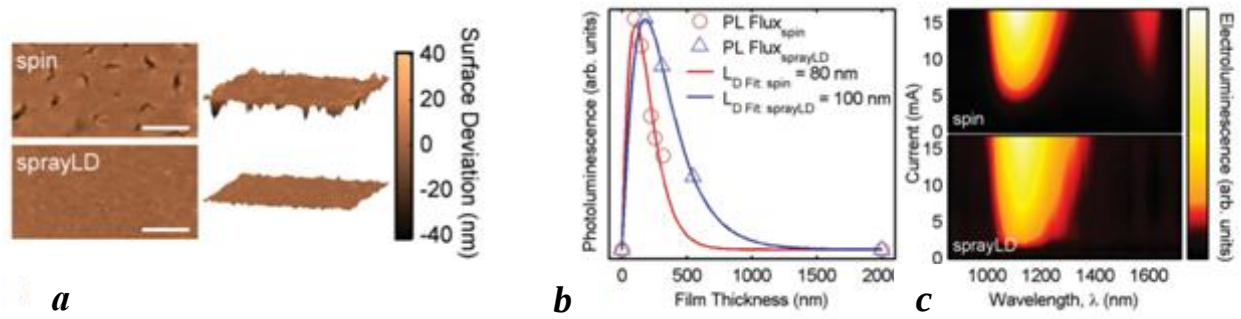


Figure 2.13 - a) Top and angled views of spin-cast films and sprayLD films obtained using AFM, b) minority carrier diffusion length measurements of spin-coated and sprayLD films and c) electroluminescence measurements of spin-coated and sprayLD films. [3]

## 2.9 Conclusions

As a result of analytical review of publications of foreign and domestic literature devoted to the synthesis of colloidal QDs and their application in solar power engineering, we can draw the following conclusions.

1) One of the most successful chemical synthesis methods of monodisperse solutions of colloidal QDs enabling to obtain high quality QDs is the hot injection method [15], the advantages of which include low temperature of synthesis and the ability to control the growth with the basic parameters.

2) Colloidal QDs are promising objects for a wide range of applications, among which solar power engineering occupies a special place. Samples of the third generation solar cells based on colloidal QDs have reached the efficiency of 8-9% [3 and 29] at the low production cost and simplicity of manufacture compared with silicon elements in a very short time.

3) One example of a successful solar panel technology is SprayLD method [3], developed in 2014, and based on spraying lead sulphide QDs. Its advantages include simplicity, applicability on the industrial scale, low cost and the possibility of creating solar cells of a large area and of different shapes.

## 3. Methodology

### 3.1 Samples with colloidal PbS QDs

To observe the efficiency of energy transfer via FRET mechanism we used non-enveloped PbS QDs synthesized by the hot injection method in this work. Within this method Pb-precursors are lead salts and organic acids and S-reagents are sulfur complexes oleylamine and the reaction medium being a mixture of octadecene, oleylamine and trioctylphosphine oxide. All reactions proceed under an argon atmosphere at the temperature of 150-300 $^{o}$C.

QD size in the solution is determined by the average value of the diameter of the nuclei is a parameter that determines the area of optical transitions in quantum dots. To transfer energy in the near-IR spectral region, two QD solutions of lead sulphide of different diameters with absorption peaks in the range of 900 to 1700 nm have been chosen. The solvent is carbon tetrachloride ($CCl_4$) because of the lack of their own absorption band in the considered spectral range in contrast to other solvents used when working with PbS QDs. Apart from the size and position of the absorption and luminescence peaks, it is important to consider the value of QD concentration in the used solvent as well as their quantum fluorescence yield.

On the basis of two stock solutions of PbS QDs of different sizes two types of samples were prepared: the first is QDs introduced in a porous matrix and the second is QDs inflicted on the glass surface.

### 3.2 Research methods

Measurements of the samples were carried out by optical spectroscopy including the absorption and luminescence spectroscopy in this work. Methods of absorption spectroscopy allow studying both the energy structure and absorbing capacity of samples as well as determining the concentration of nanocrystals in colloidal solutions, which cannot be obtained by a direct measurement. In this regard, the following algorithm is used to calculate the values of colloidal QD concentrations in solutions:

1) We have recorded the absorption spectrum of the studied QD solution, representing dependency of the density of states $D$ on the wavelength $\lambda$.

2) From the absorption spectrum we have obtained the wavelength corresponding to the first QDs exciton absorption peak and the value of optical density in this peak.

3) We have calculated the average diameter of QDs in the solution using a semi-empirical formula, depending on the wavelength value at the maximum of absorbance.

4) We have calculated extinction coefficient based on the QD type in the solution, using an appropriate empirical formula connecting the extinction coefficient and QD radius.

5) Substituting the value of the extinction coefficient and the value of the optical density in the first exciton absorption peak under Beer–Lambert–Bouguer law, we have calculated the concentration of semiconductor nanocrystals in the colloid solution.

$$I = I_0 e^{-\varepsilon Cl},\ D = \lg\left(\frac{I_0}{I}\right) = \varepsilon Cl \quad \longrightarrow \quad \varepsilon = \frac{D}{Cl} \tag{10}$$

where $D$ is optical density, $C$ is the molar concentration, $\varepsilon$ is the extinction coefficient (absorption coefficient) of the solution and $l$ is the optical path length (cuvette thickness).

In turn, the fluorescent spectroscopy is a universal non-destructive method for studying the properties of the electron subsystem of colloidal QDs. It is characterized by high sensitivity and the ability to analyze objects placed on the opaque substrates, as in the case of samples with PbS QDs in the porous matrix.

Thus, optical methods such as fluorescent and absorption spectrometry are potent and indispensable tools for the study of monodisperse colloidal QDs.

For a more complete analysis of the energy transfer process between PbS QD in the studied samples we have measured QDs luminescence decay times. The decay time of the PL represents the average time during which the QD system is in an excited state.

## 3.3 Stationary measurements

### 3.3.1 Absorption spectra

In this work, to record absorption spectra of the samples we use Shimadzu UV-3600 spectrophotometer designed to work over a wide spectral range from UV to the near infrared range (185 nm to 3300 nm). UV-3600 Spectrophotometer has both preliminary and main monochromators, each of which contains two gratings, two radiation sources and three detectors: a photomultiplier and two semiconductor detectors of InGaAs and PbS. The high sensitivity of the system in combination with a broad spectral range and different modes of operation allow

characterizing with a high degree of accuracy samples based on QDs. Figure 3.1 shows the optical scheme of the tool.

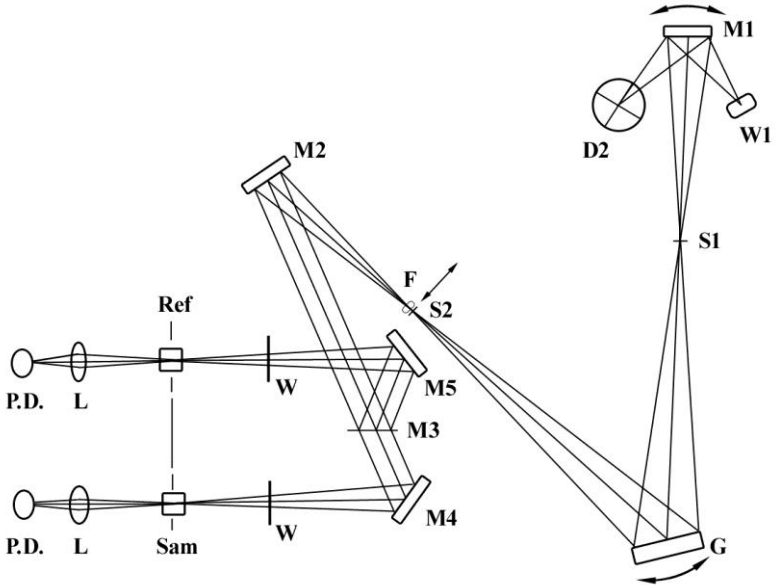


Figure 3.1 - Optical scheme of a spectrophotometer of the UV-3600 series [34].
D2 is the deuterium lamp; WI is the halogen lamp; F is the filter; G is the diffraction grids; S1 is the entrance slot; S2 is the output slot; W is the window-plates; M1-M5 are the mirrors; M3 is the half-mirror; L are the lens; Ref is the comparing channel; Sam is the sample channel and PD is the photodiode.

The spectra were recorded in the 800 nm to 2000 nm wavelength range with spectral resolution 0,1 nm. Table 3.1 presents the main technical characteristics of the UV-3600 spectrophotometer.

Table 3.1 - Technical specifications of Shimadzu UV- 3600 spectrophotometer

| | |
|---|---|
| Spectral range: | 185 nm – 3300 nm |
| Monochromator: | Czerny-Turner with the correction of aberrations;<br>diffraction grids:<br>1200 lines / mm<br>1000 lines / mm |
| Maximum spectral resolution: | 0.1 nm |
| Optical scheme: | Double beam |
| Wavelength setting tolerance: | ±0.2 nm |
| Wavelength setting repeatability: | ±0.08 nm |
| Measuring range of optical densities: | -6 to 6 |

| | |
|---|---|
| The maximum noise level:<br>500 nm<br>900 nm<br>1500 nm | <br>0.00005<br>0.00008<br>0.00003 |
| Baseline correction: | Automatic, retentive, Re-writable baseline |
| Excitation source: | 50 W halogen lamp, deuterium lamp; built-in automatic positioning of lamps in accordance with the test range |
| Radiation receiver (for the visible spectrum): | Photomultiplier “ФЭУ R928’ |

### 3.3.2 Luminescence spectra

Studies of PL spectra in the near infrared range are carried out on the original pilot plant, the use of which is conditioned by the lack of commercial equipment meeting the highest requirements used to precision fluorescent measurements [35]. Figure 3.2 shows the installation diagram.

This experimental facility is built on an Acton SP-2558 monochromator with an aperture of f/6.5, a focal length of 500 mm and a diffraction grating of 150 lines / mm. With the minimum slot width the spectral resolution is 0.4 nm. As the excitation source we use a helium-neon laser and a solid-state laser with wavelengths of 633 nm and 532 nm and a maximum power of 15 mW. A more detailed description of the main functional components of the experimental installation is in the operation manual [34], and the description of the tool calibration can be found in [36].

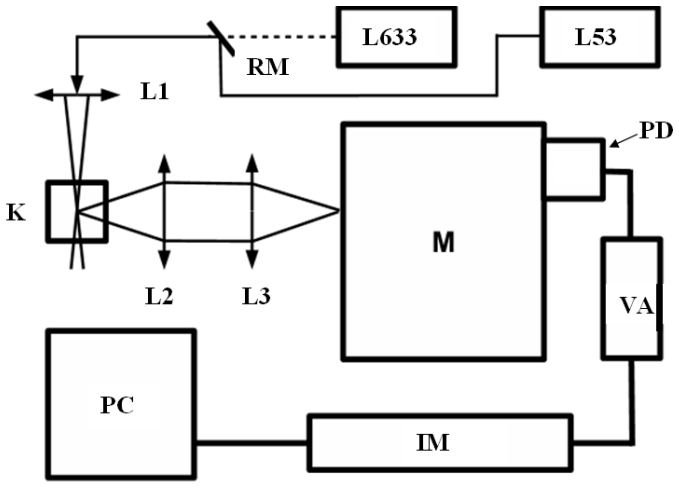


Figure 3.2 - Functional diagram of the used PL measurement setup [34].

L532, L633 are lasers (with a wavelength of 532 nm and 633 nm, respectively); L1 is the lens that focuses the laser radiation (f = 10 cm); K is the sample holder; L2, L3 are lens collecting and

focusing PL radiation (f = 25 mm and 15 cm, respectively); M is the monochromator;
RM is the reclining mirror; PD is the photodiode; VA – voltage amplifier;
IM – signal digitizing interface module and PC is the personal computer.

### 3.4 Dynamic measurements

Dynamic measurements are carried out on a setup using 90° angle between excitation and detection, which allows researching both the QDs solutions in the cuvette, and the QDs on surfaces and in thin porous matrices. Functional diagram of the installation for dynamic measurement is shown in Figure 3.3.

A solid-state pulsed laser of the model DTL-399QT model capable of generating laser radiation at three wavelengths (351 nm, 527 nm and 1053 nm) serves as a source of excitation. In the work we use laser radiation with a wavelength of 527 nm, and radiation at other wavelengths was blocked by glass filters. The pulse duration is $\approx$10 ns at a repetition rate of 4 kHz, which is set by Metex MXG-9810A, an external pulse generator. Femto HCA-S-200M-IN, a high-speed photodetector with an integrated InGaAs photodiode with a sensitive area diameter of 0.3 mm and sensitive in 0,9 μm - 1,75 μm is used as a receiver of optical radiation. Additional amplification is provided by Stanford Research SR455A, a radiofrequency amplifier with a bandwidth of 350 MHz. Registering an amplified signal is carried out by PicoScope 3206A oscilloscope with a bandwidth of 200 MHz and a sampling frequency of 500 million samples per second [37]. The time resolution of this installation is 3 ns and mainly determined by the amplifier's speed with a built-in photodiode.

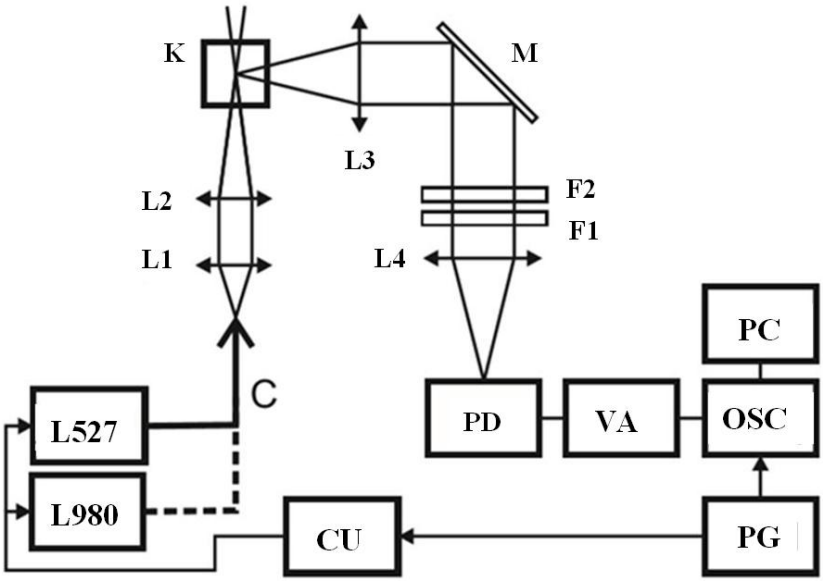


Figure 3.3 - Functional diagram of the setup for the dynamic analysis of the luminescence of nanostructures in the near infrared region of the spectrum [34].

L527 is the pulse laser; CU is the laser control unit, PG is the external pulse generator; M is the mirror; OSC is the oscilloscope; PC is the personal computer; L1- L4 are lens;

VA is the voltage amplifier; PD is the photodiode; F1,2 are filters that block the excitation radiation and K is the cuvette / sample.

## 4. Results and discussion

### 4.1 Characteristics of PbS QDs in solutions of different sizes

Lead sulphide QDs of various sizes are prepared as solutions in $CCl_4$ with a concentration of QDs is about $10^{-6}$ Mole/cm$^{-3}$. For all of the prepared solutions absorption spectra are recorded on Shimadzu UV-3600 spectrophotometer, the description of which is in Section 3.3.1 and PL spectra are measured on the original setup described in Section 3.3.2. PL decay times in colloidal solutions are measured with the setup described in Section 3.4.

Based on the data obtained from the absorption spectra we have calculated average diameters of the QDs using the semi-empirical formula [38].

$$d_{av} = 7,2 \cdot 10^{-10} \cdot \lambda^3 - 1,7 \cdot 10^{-6} \cdot \lambda^2 + 5,57 \cdot 10^{-3} \cdot \lambda - 0,9 \qquad (11)$$

where $\lambda$ is the wavelength corresponding to the center of the first interband transition in the absorption spectrum. The parameters characterizing PbS QDs in colloidal solutions are presented in Table 4.1, and the absorption and luminescence spectra and PL decay curves measured at room temperature are shown in Figures 4.1-4.6.

Table 4.1 - Characteristics of QDs in colloidal solutions.

| № | Title | Diameter, nm | Max abs, nm | Max. lum nm | **t, ms** |
|---|---|---|---|---|---|
| 1 | **PbS_925** | 3.6 | 955 | 1050 | **1.76** |
| 2 | PbS_1060 | 4.3 | 1110 | 1175 | **1.28** |
| 3 | PbS_1115 | 4.4 | 1120 | 1205 | **1.50** |
| 4 | **PbS_1180** | 4.6 | 1180 | 1270 | **1.62** |
| 5 | PbS_1380 | 5.5 | 1355 | 1130, 1410 | **1.34** |
| 6 | PbS_1640 | 6.9 | 1605 | 1615 | **0.67** |

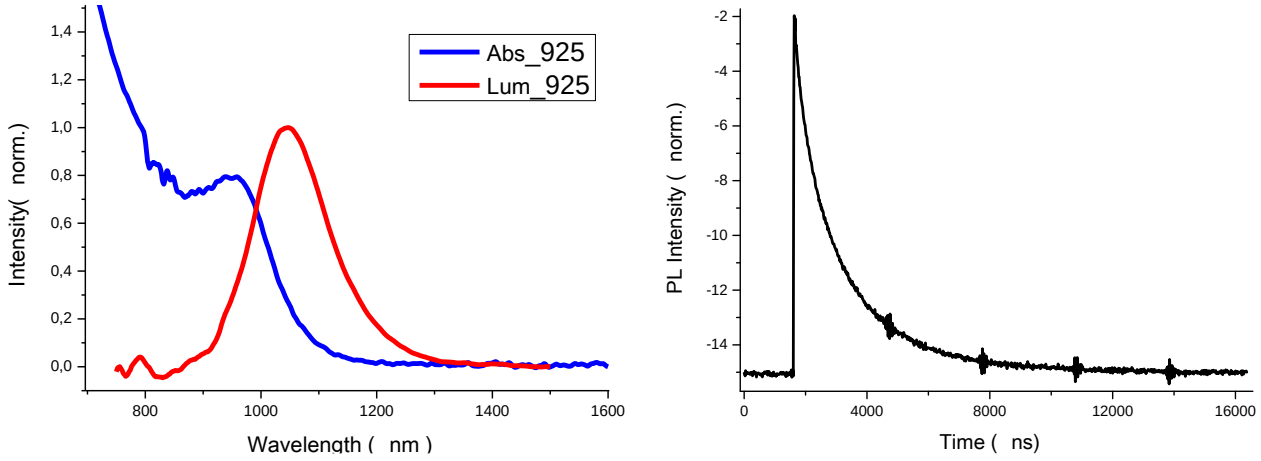


Figure 4.1 - a) Absorption and PL spectra and b) the PL decay curve for the sample PbS_925.

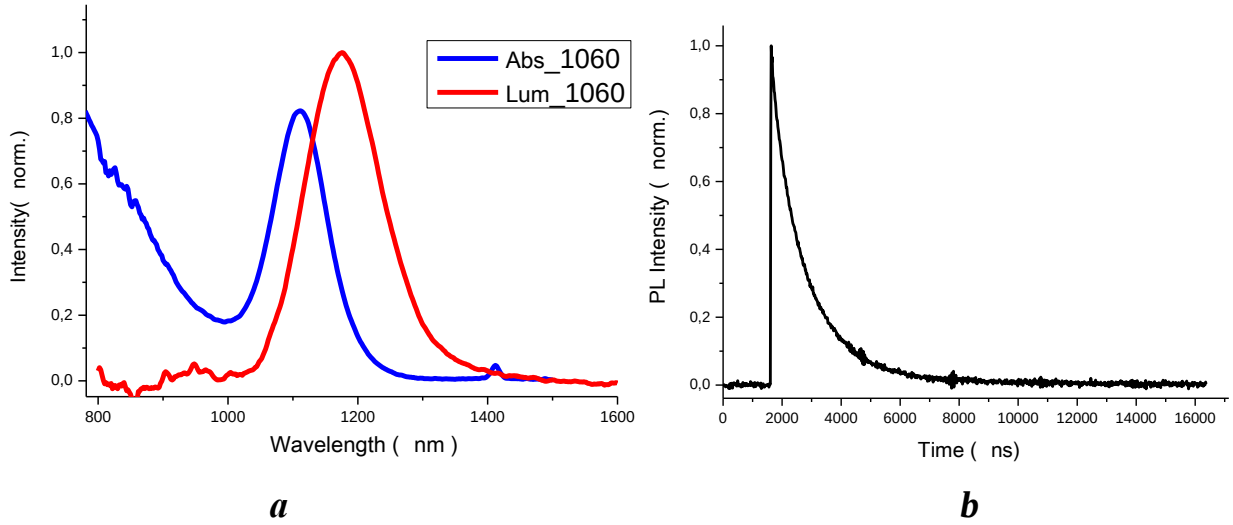


Figure 4.2 - a) Absorption and PL spectra and b) the PL decay curve for the sample PbS_1060.

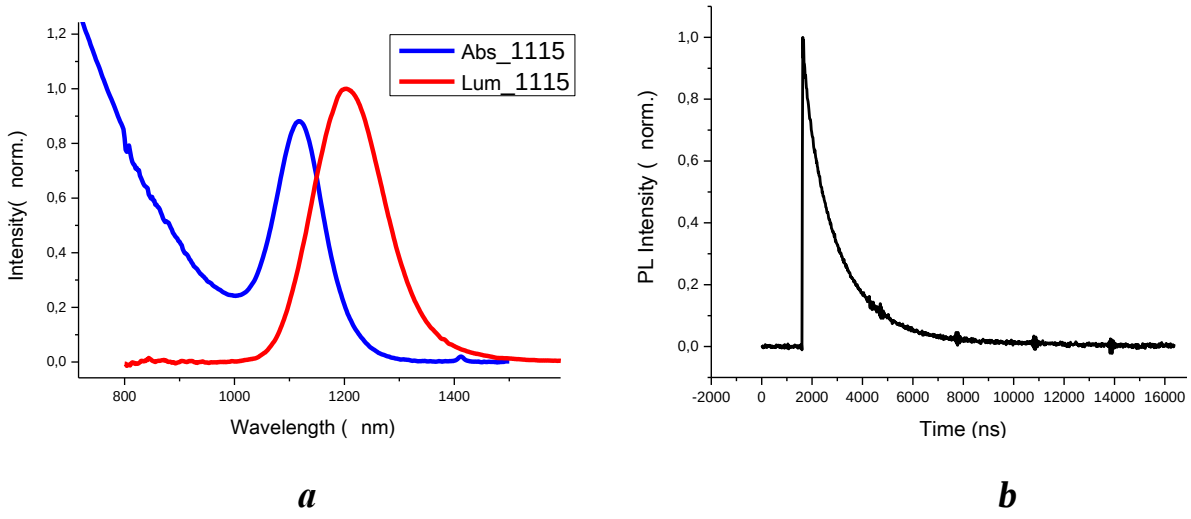


Figure 4.3 - a) Absorption and PL spectra and b) the PL decay curve for the sample PbS_1115.

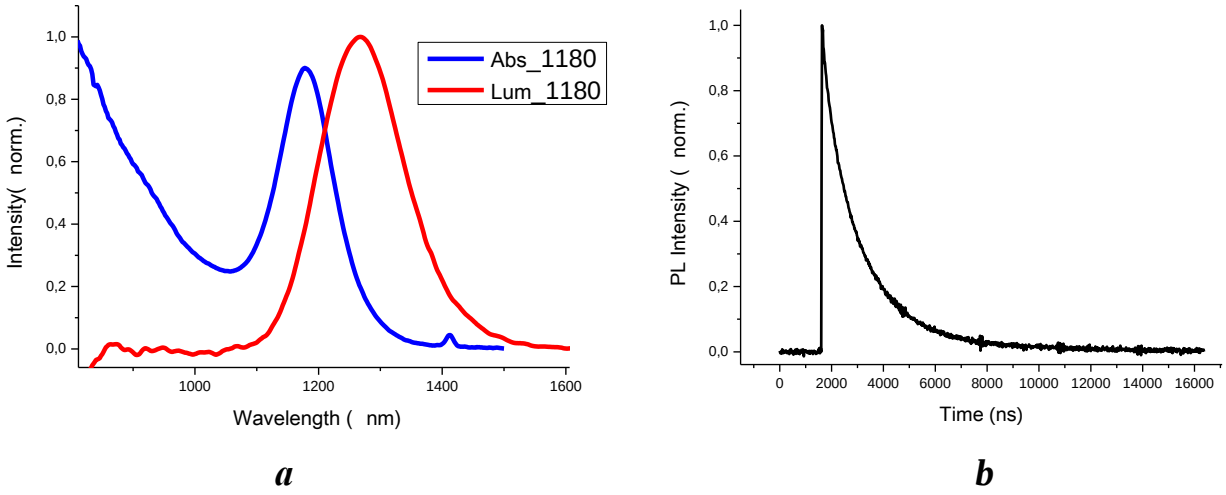


Figure 4.4 - a) Absorption and PL spectra and b) the PL decay curve for the sample PbS_1180.

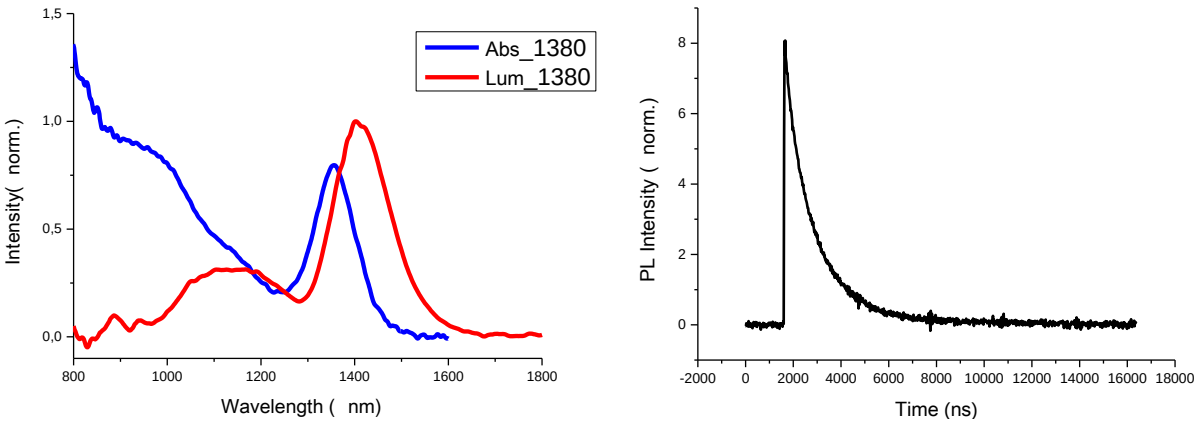


***a*** ***b***

Figure 4.5 - a) Absorption and PL spectra and b) the PL decay curve for the sample PbS_1380.

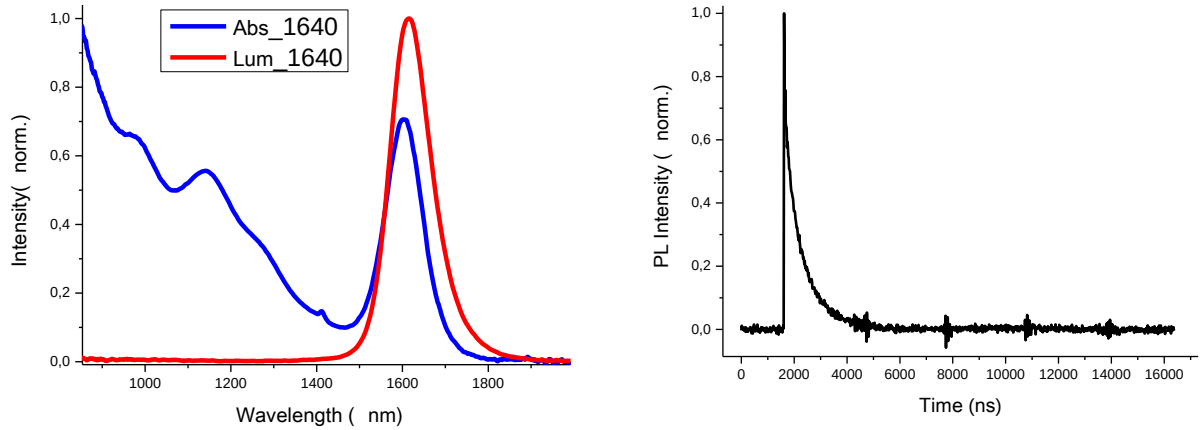


***a*** ***b***

Figure 4.6 - a) Absorption and PL spectra and b) the PL decay curve for the sample PbS_1640.

The measured lifetimes of lead sulphide QDs are in the range from 0.67 μs to 1.76 μs which is much higher than the value predicted by the theory. Furthermore, there is an abnormal dependence, which is expressed in a decrease of the luminescence lifetime of QDs with their size increasing.

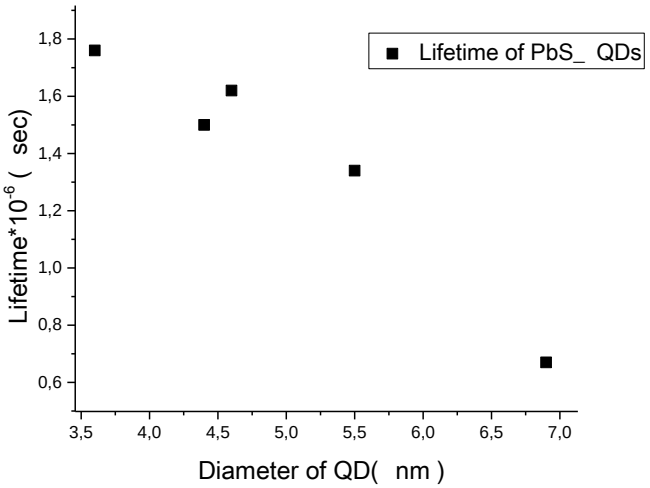


Figure 4.7 - The size dependence of the PL lifetime of PbS QDs.

Figure 4.8 shows the dependence of the maximum luminescence position on the QDs size, which shows a linear increase in the PL peak wavelength with the QDs size.

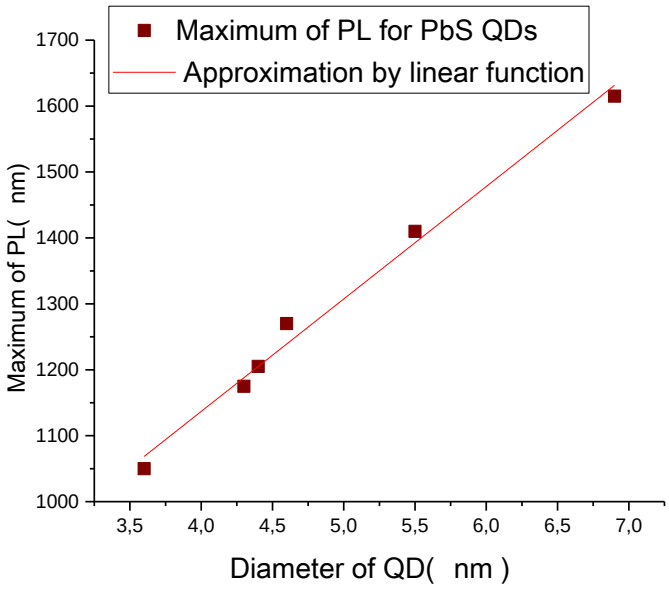


Figure 4.8 - Size dependence of the maximum PL peak position of PbS QDs.

## 4.2 Selecting a QD pair and preparing samples for research

To monitor the energy transfer via the FRET mechanism between lead sulphide QDs of different sizes as energy donors colloidal solutions with QDs of the smallest size with a diameter of 3.6 nm and the absorption peak at 955 nm are selected, and as the energy acceptor QDs with a diameter of 4,6 nm and the absorption peak at 1180 nm. The smaller type of QDs is designated as QD1 and the larger ones as QD2.

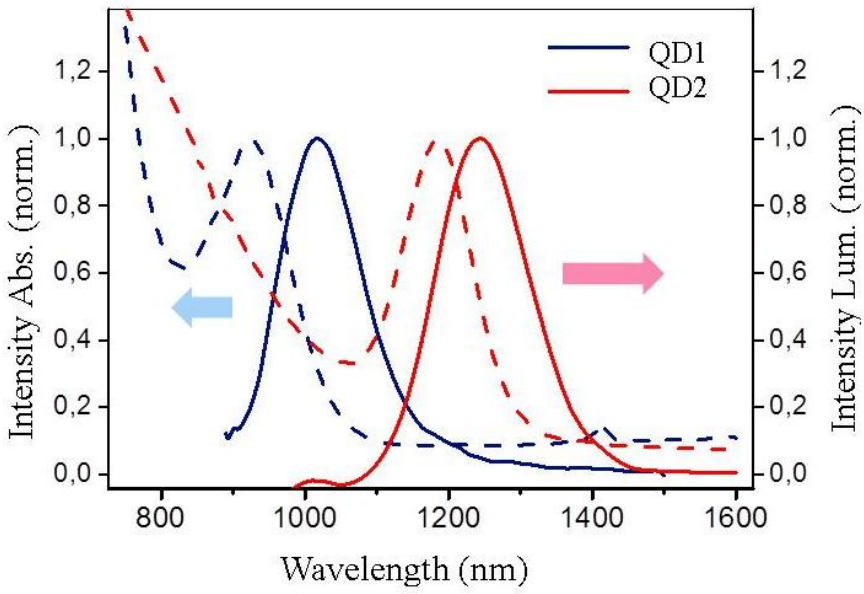


Figure 4.9 - Normalized absorption and PL spectra of the QD types QD1 and QD2.

From the overlap of the QD1 luminescence spectrum and the QD2 absorption spectrum we can conclude that the first condition required for effective monitoring of energy transfer via FRET mechanism is completed, in contrast to the second condition related to the distance between the donor points and the acceptor points. As QDs are in the colloidal solution, it is obvious that the distance between them will be significantly larger than the value of Förster radius. Ultimately, this will lead to a significant lack of energy transfer between QDs in a colloidal solution. Therefore, it was decided to prepare such samples using QD1 and QD2 colloidal solutions in which the distance between QDs would not be greater than the value of Förster radius.

To prepare the samples, we used two QD1 colloidal solutions with a concentration of $7.1*10^{-6}$ ppm and QD2 with a concentration of $3.8*10^{-6}$ ppm as well as a mixed solution containing two kinds of QDs.

Samples of the first type were PbS QDs on the glass surface, which were prepared by layering the QDs solutions on glasses which were purified by $CCl_4$. Each sample had at least six layers and each subsequent layer applied after drying of the previous.

Samples of the second-type were PbS QDs introduced in a porous matrix in which a filter paper with a thickness of 0.14 mm was used. To produce QD samples in porous matrix the filter paper was put in the QD solution for one minute and after drying was attached onto a glass slide. Figure 4.10 shows photographs of all the samples.

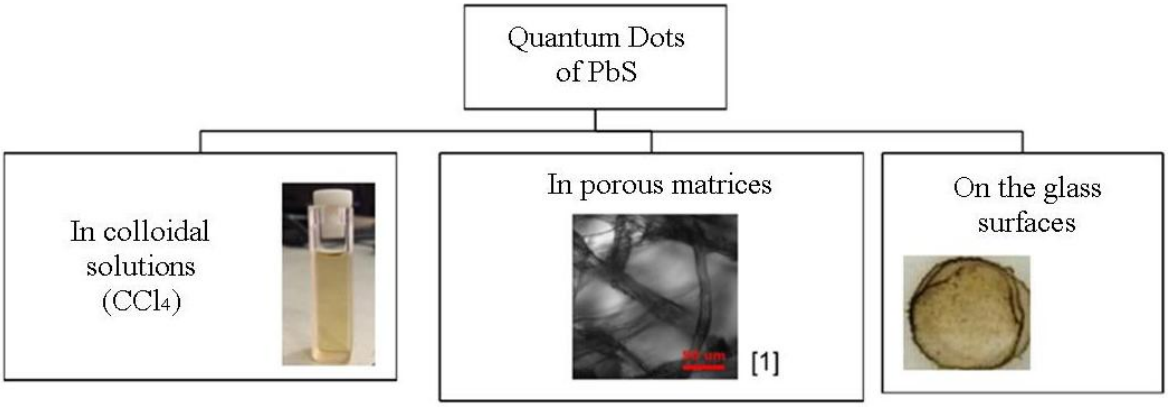


Figure 4.10 - Samples with PbS QDs and the paper structure photo with embedded QDs [39].

Table 4.2 demonstrates the structure of prepared samples with QDs.

Table 4.2 - Test samples.

| Sample | QD in solution | | | QD on the glass surface | | | QD in a porous matrix | | |
|---|---|---|---|---|---|---|---|---|---|
| | 1 | 2 | 12 | 1 | 2 | 12 | 1 | 2 | 12 |
| QD1 | + | | + | + | | + | + | | + |
| QD2 | | + | + | | + | + | | + | + |

## 4.3 Energy transfer in the PbS QD system

The efficiency of energy transfer in the system of densely packed QDs can be estimated, first, according to the extent of quenching of PL of donors using the following formula.

$$E = 1 - \frac{\tau_{DA}}{\tau_D} \tag{12}$$

where $\tau_{DA}$ is the donor lifetime in the presence of the acceptor and $\tau_D$ is the donor lifetime in a pure sample. And, secondly, it is done according to the PL quenching of the donor-points in a mixed sample, i.e., by calculating the ratio

$$n = \frac{I_{DA}}{I_D} \tag{13}$$

where $I_{DA}$ is the donor luminescence intensity in the presence of acceptors and $I_D$ is the donor luminescence intensity without the acceptors.

### 4.3.1 PL spectra

The luminescence spectra of samples with QDs with their approximation under Gaussian function are shown in Figures 4.11 - 4.13. This approximation cannot be considered optimal, but it allows us to approximately estimate the maximum intensity of individual luminescence bands.

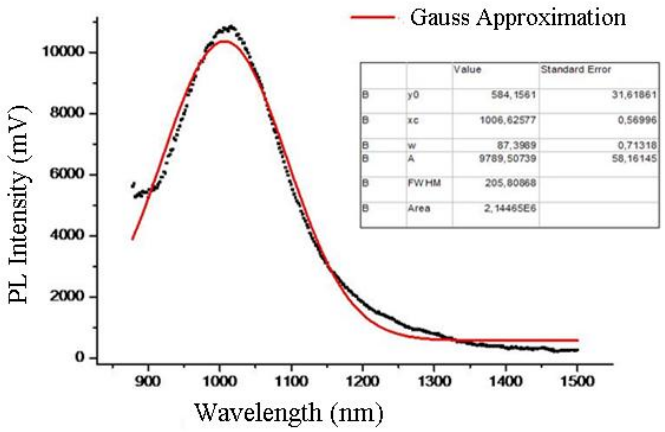


Figure 4.11 – PL spectrum for QD donors in a porous matrix with Gaussian function approximation.

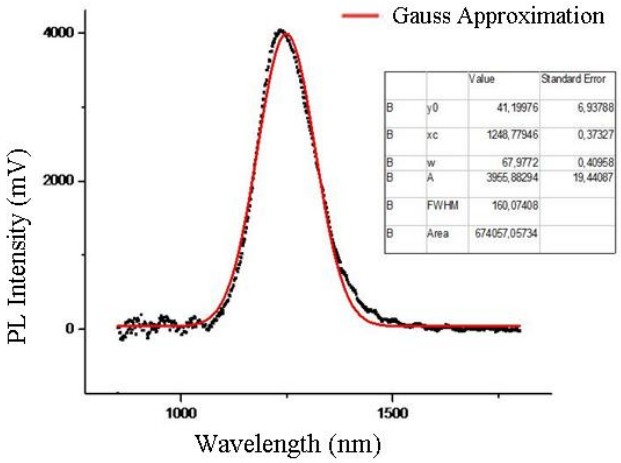


Figure 4.12 – The PL spectrum for QD acceptors in a porous matrix with Gaussian function approximation.

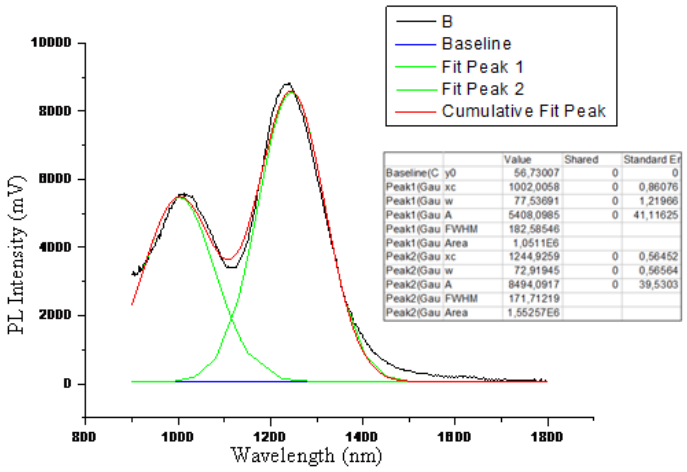


Figure 4.13 – PL spectrum for QDs in a mixed sample matrix with Gaussian function approximation.

Table 4.3 - The amplitude of the signal from various PL bands in individual samples and mixtures.

| QD /sample | In absolute units, mV | | | In relative units |
|---|---|---|---|---|
| | Sam_1 | Sam_2 | Sam_12 | Sam_12 |
| QD1 | 9790 | | 5410 | 1,8 ↓ |
| QD2 | | 3955 | 8495 | 2,1 ↑ |

Table 4.3 shows that the energy transfer in a system of densely packed QDs in the porous matrix is accompanied by donor quenching by 1.8 times during flare-up of PL acceptors in 2.1 times.

### 4.3.2 PL decay times

Decay time is recorded by allocating narrow spectral bands with the width of 40 nm using tunable filters collected on the short-focus monochromator [37]. The central wavelength for recording the PL signal from QD samples is chosen in accordance with the position of their PL peaks and is either 1050 nm or 1270 nm. The PL decay time of the mixed sample is measured similarly for each of the two luminescence bands.

The PL decay curves for the QD on the glass surface and in the porous matrix are recorded at room temperature. The measurement results are presented in Figures 4.14 - 4.15 and in Tables 4.4 - 4.5.

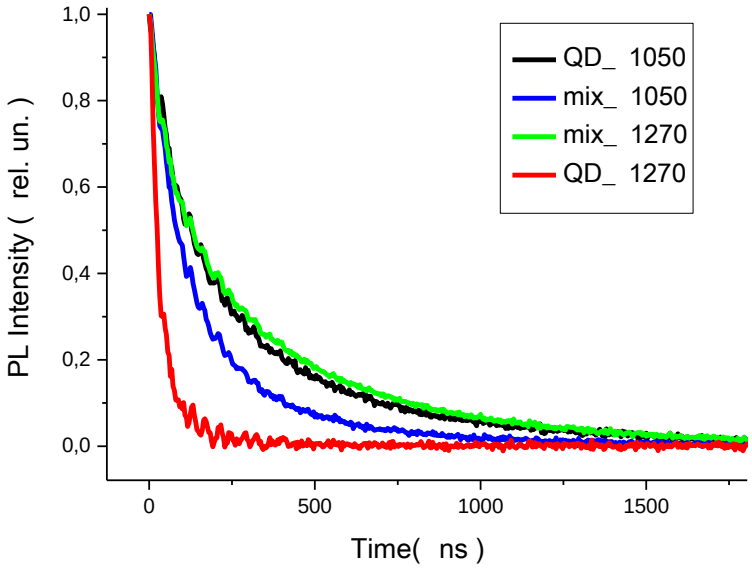


Figure 4.14 - PL decay curves of PbS QDs on the glass surface at room temperature.

Table 4.4 - The PL decay times of QDs on the glass surface.

| Curve | $A_1$ | $t_1$ | $A_2$ | $t_2$ | **t, ns** |
|---|---|---|---|---|---|
| Sam. 1 | 0,46 | 465,4 | 0,52 | 99,4 | **394** |
| Sam. 12 (1050) | 0,36 | 315,7 | 0,66 | 81,0 | **240** |
| Sam. 2 | 0,14 | 124,4 | 0,92 | 27,2 | **67** |
| Sam. 12 (1270) | 0,56 | 453,4 | 0,42 | 70,9 | **413** |

Now consider the decay curves for QDs in the porous matrix.

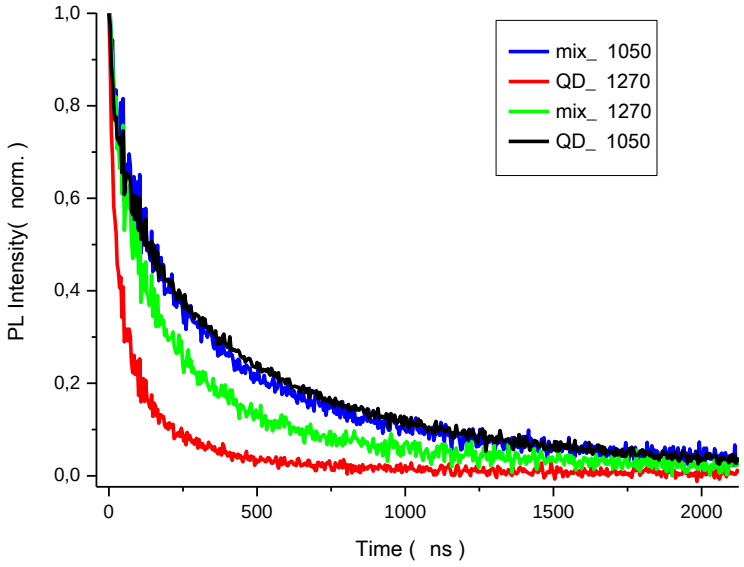


Figure 4.15 - PL decay curves of PbS QDs in the porous matrix at room temperature

Table 4.5 - The PL decay times of QDs in the porous matrix

| Curve | $A_1$ | $t_1$ | $A_2$ | $t_2$ | $A_3$ | $t_3$ | **t, ns** |
|---|---|---|---|---|---|---|---|
| Sam.1 | 0.46 | 89.6 | 0.47 | 586.4 | - | - | **520** |
| Sam.12 (1050) | 0.36 | 461.7 | 0.59 | 79.5 | - | - | **377** |
| Sam.2 | 0.66 | 25.1 | 0.30 | 204.2 | - | - | **166** |
| Sam.12 (1270) | 0.48 | 14.4 | 0.42 | 855 | 0.10 | 450.3 | **265** |

### 4.3.3 Energy transfer at decreased temperature

PL spectra are measured for the mixed sample in the porous matrix and shown in Figure 4.16 the PL spectra show that at decreased temperature the PL peaks are shifted to a longer wavelength area for both QD1 and QD2 types. Moreover, PL quenching is observed for QDs of a smaller size together with a displacement at decreasing temperature.

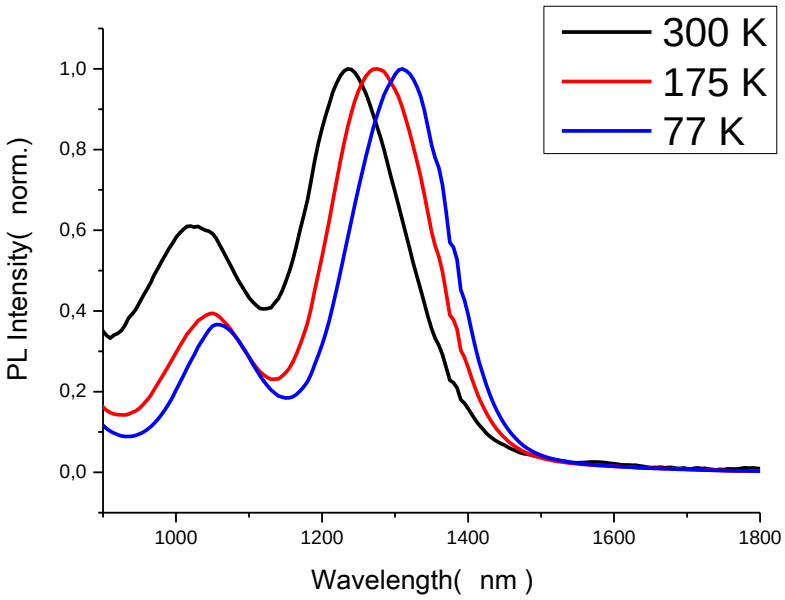


Figure 4.16 - PL spectrum for QDs in the porous matrix at three temperatures.

For a more complete analysis of the energy transfer process between QDs in the porous matrix decay times were measured at liquid nitrogen temperature. Samples with QDs were placed in a cryostat connected with the Dewar's vessel with liquid nitrogen, the sample temperature was kept constant at 77 K.

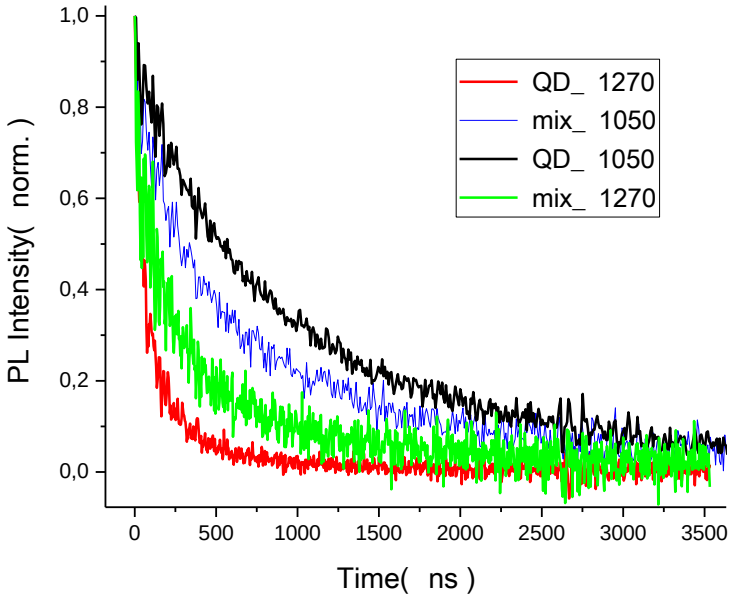


Figure 4.17 - PL decay curves of PbS QDs in the porous matrix at 77 K.

Table 4.6 contains the values of PL lifetimes with coefficients derived from the two-exponential function approximation:

$$PL = A_0 + A_1 \exp\left(-\frac{t}{t_1}\right) + A_2 \exp\left(-\frac{t}{t_2}\right) \quad (14)$$

where PL is the decay times being calculated by the following formula

$$t = \frac{A_1 t_1^2 + A_2 t_2^2}{A_1 t_1 + A_2 t_2} \quad (15)$$

where $A_1$, $A_2$ are the positive coefficients, $t_1$, $t_2$ are the time components.

Table 4.6 - PL decay times of QDs in the porous matrix at 77 K.

| Curve | $A_1$ | $t_1$ | $A_2$ | $t_2$ | **t, ns** |
|---|---|---|---|---|---|
| Sam. 1 | 0.482 | 266.3 | 0.401 | 1420.5 | **791** |
| Sam. 12 (1050) | 0.351 | 640.7 | 0.433 | 116.6 | **351** |
| Sam. 2 | 0.695 | 47.3 | 0.283 | 303.1 | **121** |
| Sam. 12 (1270) | 0.393 | 454.2 | 0.518 | 1547.5 | **1076** |

At the temperature of 77 K, the lifetime decreases of QD donors in the mixture is about 2 times, which indicates that the presence of energy transfer in the system. In addition, increase the lifetime of QD acceptors is almost 9 times.

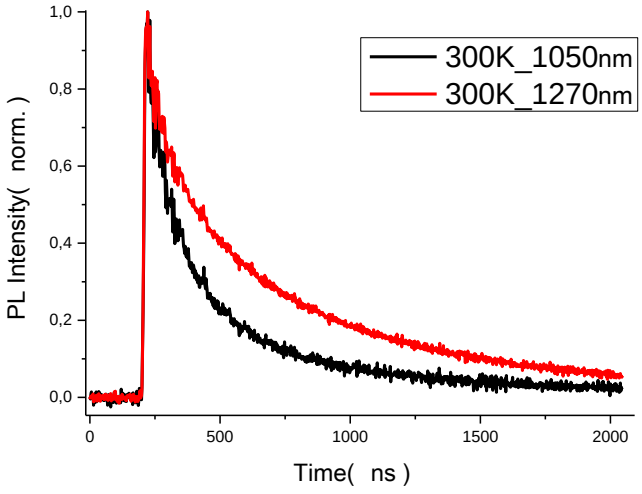


***a***

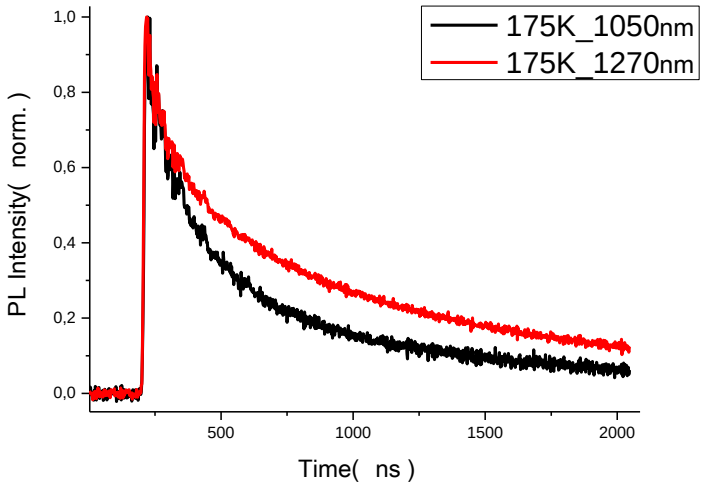


*b*

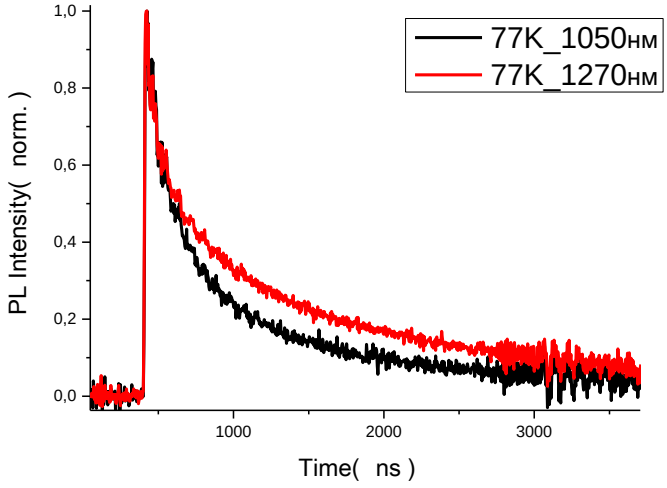


*c*

Figure 4.18 - PL decay curves for donors and acceptors in the porous matrix a) at room temperature, b) at the temperature of 175 K and c) at the temperature of 77 K.

## 4.4 Increase of the acceptor lifetime on the glass surface and in the porous matrix

Both at room temperature and at the temperatures of 77 K and 175 K a sharp increase in the lifetime of the acceptors is observed for both QDs in the porous matrix and QDs on the glass surface. This effect, in contrast to the effect of reducing the lifetime of the donors is not typical and deserves special consideration. An increase of the acceptor lifetime was observed from 67 ns to 413 ns for QDs on the glass surface at room temperature, and for QDs in the porous matrix from 166 ns to 265 ns. At the temperature of 77 K decay time of acceptors in the porous matrix increased from 121 ns to 1076 ns.

It is worth noting that in the case of QDs inflicted on the glass surface, and for QDs in the porous matrix at 77 K two exponents were enough to approximate the decay curves, i.e., they are described by the function

$$PL = A_0 + A_1 \exp\left(-\frac{t}{t_1}\right) + A_2 \exp\left(-\frac{t}{t_2}\right) \tag{16}$$

which goes well with the existing theoretical model. While for the QDs in the porous matrix at room temperature, only three decay curves could be approximated by two-exponential function, and for a curve describing luminescence of QDs acceptors, the best approximation is achieved by a three-exponential function

$$PL = A_0 + A_1 \exp\left(-\frac{t}{t_1}\right) + A_2 \exp\left(-\frac{t}{t_2}\right) + A_3 \exp\left(-\frac{t}{t_3}\right) \tag{17}$$

Table 4.7 - Comparison of approximations for QDs mixture in the porous matrix.

| $PL = A_0 + A_1 \exp\left(-\frac{t}{t_1}\right) + A_2 \exp\left(-\frac{t}{t_2}\right)$ | $PL = A_0 + A_1 \exp\left(-\frac{t}{t_1}\right) + A_2 \exp\left(-\frac{t}{t_2}\right) + A_3 \exp\left(-\frac{t}{t_3}\right)$ |
|---|---|
| 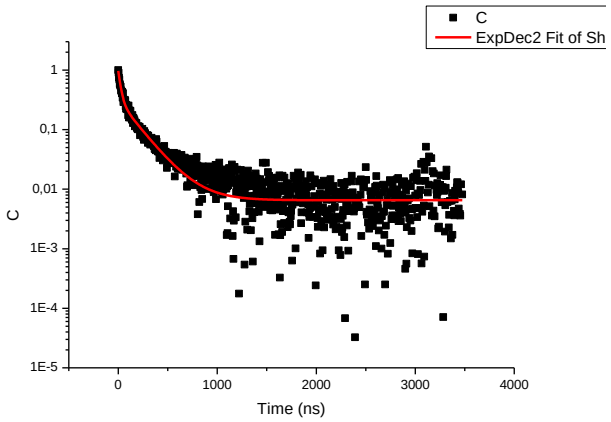 | 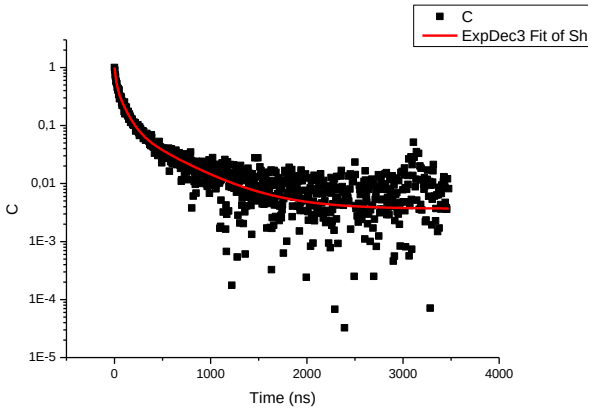 |
| 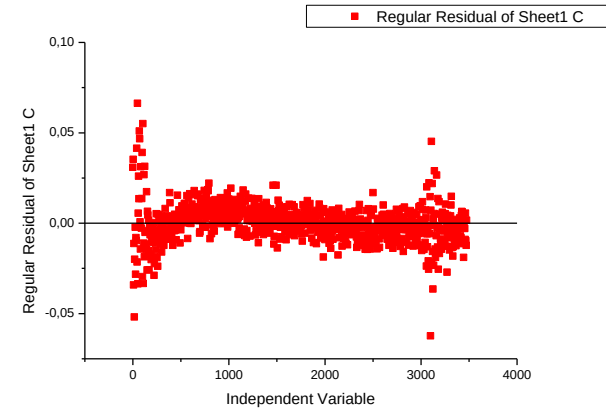 | 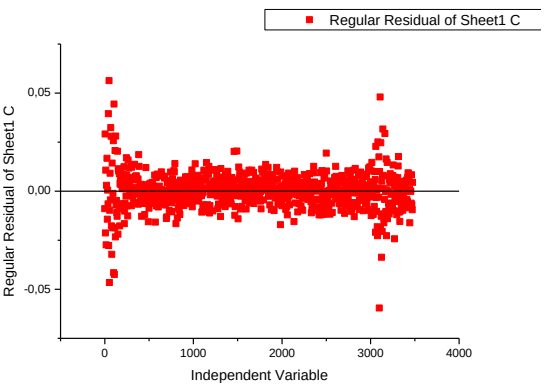 |

| | Value of | Standard Error | | Value of | Standard Error |
|---|---|---|---|---|---|
| C y0 | 0,00652 | 4,11855E-4 | C y0 | 0,00367 | 5,07241E-4 |
| C A1 | 0,66145 | 0,00915 | C A1 | 0,48166 | 0,01852 |
| C t1 | 25,07738 | 0,68715 | C t1 | 14,39887 | 0,82676 |
| C A2 | 0,30112 | 0,00755 | C A2 | 0,42438 | 0,01487 |
| C t2 | 204,15865 | 4,89443 | C t2 | 85,48163 | 5,01285 |
| | | | C A3 | 0,09923 | 0,00998 |
| | | | C t3 | 450,30166 | 35,00609 |
| **t =166 ns** | | | **t =265 ns** | | |

It is evident that the function containing three exponents provides a better approximation of the acceptor decay curve.

### 4.5 Three-level model

The observed effect of a sharp increase in the acceptor lifetime both for the samples at room temperature and for the QDs in the porous matrix at decreased temperatures can be interpreted in the framework of the three-level model. This model is based on a complex energy structure of lead sulphide QDs, which contains special long-lived states within the band gap. Since these states are involved in the energy transfer, PL decay of acceptors is determined by a long donor lifetime.

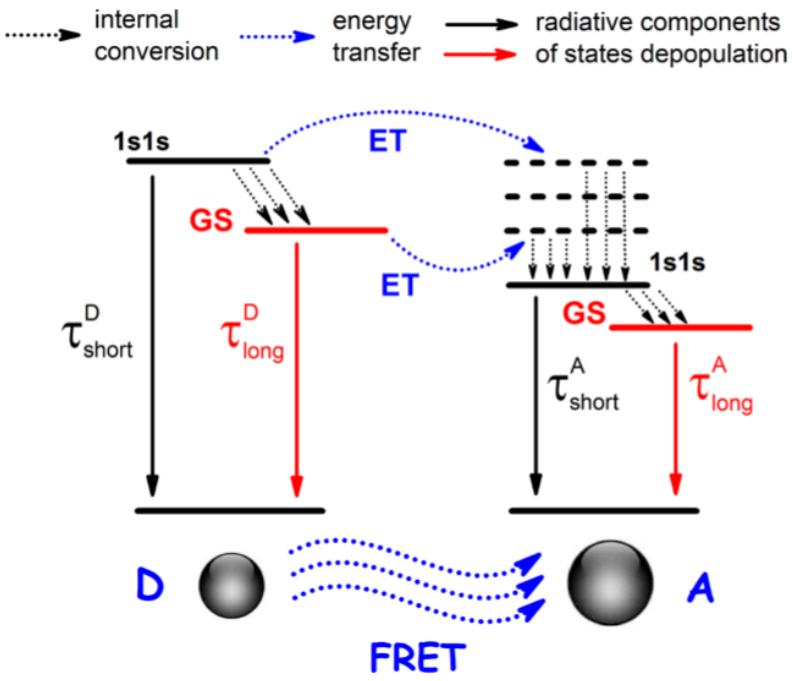


Figure 4.19 - Diagram of the electronic structure of PbS QDs of different sizes [40], the blue dotted arrows illustrate possible ways of energy transfer.

PL decay of pure QDs entered into the porous matrix can be approximated by the sum of two exponents with slow and fast component

$$PL = A_1 \exp\left(-\frac{t}{t_{long}}\right) + A_2 \exp\left(-\frac{t}{t_{short}}\right) \tag{18}$$

PL decay of acceptors should be described by a sum of four exponents, two of which are related to their own acceptor decay, and the other two are associated with the donor decay in the presence of the acceptor. However, the fast component of the donor decay should not affect the disintegration of the acceptor, so the final formula that describes the decay in the acceptor consists of the sum of three summands

$$PL^A = A_1 \exp\left(-\frac{t}{\tau^A_{long}}\right) + A_2 \exp\left(-\frac{t}{\tau^A_{short}}\right) + A_3 \exp\left(-\frac{t}{\tau^D_{long}}\right) \tag{19}$$

where the last member corresponds to the long component in the donor decay in the presence of the acceptor. These three exponents can be initially determined from the corresponding decay curves, that is, from the curve for pure donors, pure acceptors and donors in the presence of acceptors.

Thus, the three-level model allows us to explain the effect of a sharp increase in the lifetime of the acceptors to the values characteristic of the QD-donors for PbS QDs in the porous matrix.

## 5. Conclusion

In this thesis we have studied the process of nonradiative energy transfer via the FRET mechanism between lead sulphide QDs with the diameter of 3.6 nm and 4.6 nm in the porous matrix and on the glass surface at room temperature and at decreased temperatures.

For QDs in the porous matrix studied at liquid nitrogen temperature, we have observed quenching of donor QDs by 2 times during the flare-up of PL of acceptor QDs by almost 9 times. In addition, we have observed a shift of the PL peaks for the two types of QDs when decreasing the sample temperature from room temperature to 77 K.

At room temperature for QDs on the glass surface we have detected PL quenching of donors by 1.6 times and increase of the acceptor lifetime by 6.1 times. For QDs in the porous matrix we have observed PL quenching of donors by 1.8 times and the flare-up of PL of acceptor QDs by 2.1 times. In contrast to the glass samples, PL of acceptor-dots in the porous matrix is described by three exponents. The need for an additional exponent in the approximation has been explained in the framework of the three-level model, which considers the specific long-lived states of donor QDs from which the energy is transferred to the acceptor QDs.

Thus, we have found out a significant PL slowdown both in the samples with QDs inflicted in the porous matrix and in the samples with QDs on the glass surface, as well as a sharp increase in the PL of acceptor QDs. The observed effect of increasing the lifetime of the lower electronic states of QD system can lead to a significant change in the dynamic characteristics of the charge carriers in the third generation solar cells, for example, based on QD spray technology applied on various surfaces.

**References**


1. REN21. Key Findings // Glob. Status Rep. – 2015. – C. 1–33.
2. REN21. The First Decade: 2004-2014, 10 Years of Renewable Energy Progress // Annual Rep. – 2014. – C. 1 – 48.
3. Kramer I.J., Minor J.C., Moreno-Bautista G., Rollny L. et al. Efficient spray-coated colloidal quantum dot solar cells // Adv. Mater. – 2014. – Vol. 27, № 1. – P. 116 –121.
4. V. Till. Inkjet decoration of curved surfaces at high capacities: Challenges and successful implementation, IMI Europe Conference, Lisbon, Portugal, 2013, November 13 – 15.
5. Søndergaard R., Hösel M., Angmo D., Larsen-Olsen T. et al. Roll-to-roll fabrication of polymer solar cells // Mater. Today. – 2012. – Vol. 15, № 1-2. P. 36 – 49.
6. А.В. Федоров, И.Д. Рухленко, А.В. Баранов, С.Ю. Кручинин. Оптические свойства полупроводниковых квантовых точек. – СПб.: Наука, 2011. – С. 9 – 11.
7. Карпов С.В., Микушев С.В. Электрон-дырочные возбуждения в квантовых точках CdSe в условиях сильного и промежуточного конфайнмента // Физика твердого тела. – 2003. – Т. 52, №8. – С. 1627–1633.
8. Speirs M.J., Balazs D.M., Fang H.H., Lai L.-H et al. Origin of the increased open circuit voltage in PbS–CdS core–shell quantum dot solar cells // J. Mater. Chem. A. – 2015. – Vol. 3, № 4. – P. 1450 – 1457.
9. Васильев Р.Б., Дирин Д.Н. Квантовые точки: синтез, свойства, применение. М.: 2007. ФНМ, С. 3 – 12.
10. Klimov V.I. Optical Nonlinearities and Ultrafast Carrier Dynamics in Semiconductor Nanocrystals // Phys. Chem. B. – 2000. – №104. – P. 6112-6123.
11. Förster T. Energy transfer with special reference to biological systems. 10th spiers memorial lecture transfer mechanisms of electronic excitation // Discuss. of the Faraday Soc. – 1959 – Vol. 27, № 27. P. 1 – 29.
12. Rogach A.L., Klar T.A., Lupton J.M., Meijerink A. et al. Energy transfer with semiconductor nanocrystals / // Mater. Chem. – 2009. – Vol. 19, № 9. – P. 1208 –1221.
13. Tabassum S., Al-Asbahy W.M., Afzal M., Arjmand F. et al. Interaction and photo-induced cleavage studies of a copper based chemotherapeutic drug with human serum albumin: spectroscopic and molecular docking study // Mol. BioSystems. – 2012. – № 8. – P. 2424 – 2433.
14. Минько Н., Строкова В., Жерновский И., Нарцев В. Методы получения и свойства нанообъектов. – М.: Флинта Наука, 2009. – С. 15 – 19.

15. Murray C.B., Norris D.J., Bawendi M.G. Synthesis and characterization of nearly monodisperse CdE (E = S, Se, Te) semiconductor nanocrystallites // J. Am. Chem. Soc. – 1993. – Vol. 115, № 4. – P. 8706 – 8715.

16. Murray C.B., Kagan C.R. Synthesis and Characterization of Monodisperse Nanocrystals and Close-Packed Nanocrystal Assemblies // Annu. Rev. Mater. Sci. – 2000. – № 30. – P. 545 – 610.

17. Bullen C. R., Mulvaney P. Nucleation and Growth Kinetics of CdSe Nanocrystals in Octadecene // Nanoletters. – 2004. – Vol. 4, № 12. – P. 2303-2307.

18. Sargent E. H. Colloidal Quantum Dot Optoelectronics and Photovoltaics. – NY.: Cambridge University Press, 2013. – P. 17-20.

19. Margeat, Amiens C., Chaudret B., Lecante P. et al. Chemical control of structural and magnetic properties of Cobalt nanoparticles // Chemistry of Materials. – 2005. – № 17. – P. 107 – 111.

20. Dumestre F., Chaudret B., Amiens C., Renaud P. et al. Superlattices of Iron nanocubes synthesized from Fe[N(SiMe3)2]2 // Science. – 2004. – № 303. – P. 821 – 823.

21. Desvaux C., Amiens C., Fejes P., Renaud P. et al. Multimillimetre-large superlattices of air-stable iron–cobalt nanoparticles // Nature Materials. – 2005. –Vol. 4. – P. 750 – 753.

22. Hickey S.G., Waurisch C., Rellinghaus B., Eychmüller A. Size and shape control of colloidallysynthesized IV–VI nanoparticulate tin (II) sulfide // J. of the American Chem. Soc. – 2008. – Vol. 130, № 45. – P. 14978 – 14980.

23. Baumgardner W. J., Choi J.J., Lim Y-F., Hanrath T. SnSe nanocrystals: synthesis, structure, optical properties, and surface chemistry // J. of the American Chem. Soc. – 2010. – Vol. 132. – P. 9519 – 9521.

24. Arachchige I.U., Kanatzidis M.G. Anomalous bandgap evolution from band inversion in PbSnTe nanocrystals // Nano Letters. – 2009. Vol. 9, № 4. – P. 1583–1587.

25. Glaria A., Kahn M.L., Lecante P., Barbara B. et al. $Fe_{1-y}O$ nanoparticles: organometallic synthesis and magnetic properties / Glaria // Chemphyschem – 2008. – № 9. – P. 776 – 780.

26. Green M.A., Emery R., Hishikawa Y., Warta W. et al. Solar cell efficiency tables (version 47) // Prog. Photovolt.: Res. Appl. – 2016. – Vol. 24. – P. 3 – 11.

27. Shockley W., Queisser H.Q. // J. Appl. Phys., – 1961. – Vol. 32. – P. 510.

28. O'Regan B., Grätzel M. A low-cost, high-efficiency solar cell based on dye-sensitized colloidal TiO2 films // Nature. – 1991. – Vol. 353. P. 737 – 740.

29. Nikolenko L.M., Razumov V.F. Colloidal quantum dots in solar cells // Russ. Chem. Rev. – 2013. – Vol.82. – P. 429 – 448.

30. Sariciftci N.S., Smilowitz L., Heeger A.J., Wudi F. Photoinduced electron transfer from a conducting polymer to buckminsterfullerene // Science. – 1992. – Vol. 258. – P. 1474 – 1476.
31. H. Fu, S.-W. Tsang. Infrared colloidal lead chalcogenide nanocrystals: Synthesis, properties, and photovoltaic applications // Nanoscale. – 2012. – Vol .4, P.2187 – 2201.
32. Schaller R.D., Sykora M., Pietryga J.M., Klimov V.I. Seven excitons at a cost of one: Redefining the limits for conversion efficiency of photons into charge carriers // Nano Lett. – 2006. – Vol. 6, № 3. P. 424 – 429.
33. Schaller R.D., Sykora M., Pietryga J.M., Klimov V.I.For the bright future-bulk heterojunction polymer solar cells with power conversion efficiency of 7.4% / B.Y. Liang, Z. Xu, J. Xia et al. // Adv. Mater. – 2010. – Vol. 22. – P. 135 – 138.
34. Баранов А.В., Виноградова Г.Н., Воронин Ю.М и др.Техника физического эксперимента в системах с пониженной размерностью. Часть 2. – СПб.: СПбГУ ИТМО, 2011. С. 8 –10, С. 40 – 42.
35. Парфёнов П.С., Баранов А.В.,. Вениаминов А.В, Орлова А.О. Комплекс для люминесцентного анализа макро- и микрообразцов в ближнем инфракрасном диапазоне // Оптический журнал. – 2011. – Т. 78, №2. С. 48 – 52.
36. Parfenov P.S., Litvin A.P, Baranov A.V., Veniaminov A.V. et al. Calibration of the Spectral Sensitivity of Instruments for the Near Infrared Region // J. Appl. Spectrosc. – 2011. – Vol. 78, № 3. – P. 433 – 439.
37. Парфенов П.С. Техника физического эксперимента. – СПб.: СПбГУ ИТМО, 2015. – С. 69 – 71.
38. Ushakova E.V. Proc. 14th Int. Conf. "Laser Optics 2010", РИЦ ГУАП Санкт-Петербург, 2010, ThR6, – P. 11.
39. Litvin A.P., Ushakova E.V., Parfenov P.S, Fedorov A.V. et al. FRET between Close-Packed Quasi-Monodispersed PbS QDs in a Porous Matrix // J. Phys. Chem. C. – 2014. – Vol. 118, № 12. – P 6531 – 6535.
40. Litvin A.P., Parfenov P.S., Ushakova E.V., Vorsina T.A. et al.FRET-Activated Delayed PLuorescence in Densely Packed PbS Quantum-Dot Ensembles // J. Phys. Chem. C. – 2015. –Vol. 119. – P. 17016 – 17032.